

Muon Spin Relaxation Study of (La, Ca)MnO₃

R. H. Heffner and J. E. Sonier

MS K764, Los Alamos National Laboratory, Los Alamos, New Mexico 87545

D. E. MacLaughlin

Department of Physics, University of California, Riverside, California 92521-0413

G. J. Nieuwenhuys

Kamerlingh Onnes Laboratorium, Leiden University, 2300 RA Leiden, The Netherlands

G. M. Luke

McMaster University, Hamilton, Ontario, L8P 4N1 Canada

Y. J. Uemura

Department of Physics, Columbia University, New York, New York 10027

William Ratcliff II and S-W. Cheong

Department of Physics and Astronomy, Rutgers University, Piscataway, NJ 08854

G. Balakrishnan

University of Warwick, Coventry CV4 7AL, UK

(Draft date October 30, 2018)

Abstract

We report predominantly zero field muon spin relaxation measurements in a series of Ca-doped LaMnO_3 compounds which includes the colossal magnetoresistive manganites. Our principal result is a systematic study of the spin-lattice relaxation rates $1/T_1$ and magnetic order parameters in the series $\text{La}_{1-x}\text{Ca}_x\text{MnO}_3$, $x = 0.0, 0.06, 0.18, 0.33, 0.67$ and 1.0. In LaMnO_3 and CaMnO_3 we find very narrow critical regions near the Néel temperatures T_N and temperature independent $1/T_1$ values above T_N . From the $1/T_1$ in LaMnO_3 we derive an exchange integral $J = 0.83$ meV which is consistent with the mean field expression for T_N . All of the doped manganites except CaMnO_3 display anomalously slow, spatially inhomogeneous spin-lattice relaxation below their ordering temperatures. In the ferromagnetic (FM) insulating $\text{La}_{0.82}\text{Ca}_{0.18}\text{MnO}_3$ and ferromagnetic conducting $\text{La}_{0.67}\text{Ca}_{0.33}\text{MnO}_3$ systems we show that there exists a bi-modal distribution of μSR rates λ_f and λ_s associated with relatively ‘fast’ and ‘slow’ Mn fluctuation rates, respectively. A physical picture is hypothesized for these FM phases in which the fast Mn rates are due to overdamped spin waves characteristic of a disordered FM, and the slower Mn relaxation rates derive from distinct, relatively insulating regions in the sample. Finally, likely muon sites are identified, and evidence for muon diffusion in these materials is discussed.

PACS numbers: 71.27.+a, 72.15.Qm, 76.75.+i, 75.30.Mb

I. INTRODUCTION

The strong coupling of the spin, charge and lattice degrees of freedom in the colossal magnetoresistive (CMR) manganites gives rise to a wide variation in ground-state behavior, including paramagnetism, ferro- and antiferromagnetism, charge ordering (CO), and insulating and conducting charge transport¹. The earliest studies of these systems^{2,3} involved the substitution of a divalent alkaline earth ($R = \text{Sr}, \text{Ca}, \text{Ba}$) for trivalent La in the perovskite structured LaMnO_3 , an insulating antiferromagnet. This substitution produces a hole at a Mn site (i.e., Mn^{3+} changes to Mn^{4+}) which can hop between Mn ions with different valence states via the ferromagnetic double exchange (DE) interaction⁴. Linkage between the DE interaction and charge mobility provided an early explanation of the paramagnetic/insulating to ferromagnetic/conducting transition in $\text{La}_{1-x}\text{R}_x\text{MnO}_3$. More recent experiments⁵ and subsequent theoretical analyses⁶ have also established the importance of the local Jahn-Teller (JT) structural perturbation in the Mn^{3+} state. Thus, both the JT and DE interactions are important in determining the ground state properties and magnetic ordering temperatures in these materials. The JT and DE interactions are also thought to induce the formation of magnetoelastic polarons, local structural distortions surrounded by polarized Mn spins, in CMR compounds. The degree of polaron formation depends upon the degree of cation size mismatch between the La atom and the alkaline earth atom.⁷ Sr produces the least distortion and Ba the most. These concepts comprise the fundamental ideas behind the strong coupling of spin, charge and lattice degrees of freedom in CMR materials. In this paper we study the spin dynamics of the $\text{La}_{1-x}\text{Ca}_x\text{MnO}_3$ system using the muon spin relaxation (μSR) technique,⁸ thus providing a valuable complement to other experiments probing the charge and lattice degrees of freedom in these materials.

The $\text{La}_{1-x}\text{Ca}_x\text{MnO}_3$ system has been extensively studied because it exhibits a wide variety of ground states as a function of x below room temperature.⁹ At temperatures below about 700 K the system is orthorhombic for all Ca concentrations. The end members LaMnO_3 and CaMnO_3 are both antiferromagnetic (AFM) insulators with different magnetic structures. The addition of Ca to LaMnO_3 produces a canted AFM insulating state for $0 < x \lesssim 0.07$, a ferromagnetic (FM) insulating state (followed by CO at lower temperatures) for $0.07 < x \lesssim 0.21$, and a FM metallic state for $0.21 < x \lesssim 0.50$. Above $x = 0.50$ the system remains insulating with a high temperature CO transition observed for $0.50 \leq x \lesssim 0.875$, followed by AFM at lower temperatures. Experimentally, transport measurements¹⁰ are consistent with the formation of magnetoelastic polarons in the paramagnetic state of $\text{La}_{1-x}\text{Ca}_x\text{MnO}_3$, and both neutron scattering¹¹ and x-ray fine structure analysis¹² find evidence for the persistence of JT distortions significantly below the FM transition. Neutron scattering has been used to study the low-temperature magnetic properties in FM perovskites,¹³ and has revealed a broad peak centered around zero energy transfer which coexists with Mn spin waves near T_C .¹⁴

A. μSR experiments and data analysis

The μSR technique employed here involves the interstitial implantation of positive muons with essentially 100% spin polarization, oriented antiparallel to the initial muon momentum vector. The μ^+ decays with a mean lifetime τ_μ of 2.2 μs into a positron and two

undetected neutrinos. The positron is emitted preferentially along the muon spin direction; detection of the positron emission rate in counters aligned along the initial muon spin direction allows one to monitor the time rate of decay of the muon spin polarization along its initial spin direction. The positron emission rate dN/dt is given by

$$dN/dt = B + N_0(1/\tau_\mu) \exp(-t/\tau_\mu)[1 \pm AG_z(t)], \quad (1)$$

where B is a background (usually independent of time), N_0 is a normalization factor, A is the average asymmetry of the decay angular distribution (typically 0.2–0.3), and $G_z(t)$ describes the time rate of decay of the muon spin polarization. The $+$ or $-$ signs are appropriate for positron counters in the direction of, or opposite to, the muon spin, respectively.

The μ SR data presented here were taken at the M20 muon channel at TRIUMF (Vancouver, Canada) and on the GPS spectrometer at the Paul Scherrer Institute (Villigen, Switzerland). These data could be fit to a relaxation function $G_z(t) = G_{\text{osc}}(t) + G_{\text{rlx}}(t)$, corresponding to oscillating and relaxing terms, respectively. In zero applied field the oscillating component $G_{\text{osc}}(t)$ occurs in a magnetically ordered state and is given by

$$G_{\text{osc}}(t) = \sum_i (A_{\text{osc}})_i \exp(-t/T_{2i}) \cos(2\pi\nu_{\mu i}t + \phi_{\mu i}), \quad (2)$$

where $(A_{\text{osc}})_i$ is the amplitude of the i^{th} precessing component, $\phi_{\mu i}$ is a phase angle and $\nu_{\mu i}$ and $1/T_{2i}$ are the corresponding muon precession frequency and inhomogeneous damping rate. We define $\sum_i (A_{\text{osc}})_i \equiv A_{\text{osc}}$. The existence of multiple components can be due to more than one muon lattice site and/or different microscopic magnetic environments (even for a single muon lattice site). The quantity $2\pi\nu_{\mu i} = \gamma_\mu B_i$, with γ_μ the muon gyromagnetic ratio (8.54×10^4 Hz/Oe) and B_i the local magnetic field.

In our experiments the relaxing component $G_{\text{rlx}}(t)$ frequently approximates a stretched-exponential form:

$$G_{\text{rlx}}(t) = A_{\text{rlx}} \exp[-(t/T_1)^K], \quad (3)$$

where $1/T_1$ is a characteristic spin-lattice relaxation rate. The polycrystalline averages of A_{rlx} and A_{osc} in a magnetically ordered state (where both A_{rlx} and A_{osc} are non-zero) are $A_{\text{rlx}} = 1/3$ and $A_{\text{osc}} = 2/3$. For rapid fluctuations the muon relaxation rate $1/T_1$ is given by $1/T_1 \propto \gamma_\mu^2 \sum_q |\delta B(q)|^2 \tau(q)$, where $|\delta B(q)|$ is the amplitude of the fluctuating local field and $\tau(q)$ is the Mn-ion correlation time. The sum over the characteristic momenta q of the Mn-ion excitations occurs because the muon is a local probe. When the exponent $K < 1$ in Eq. (3) a distribution of $1/T_1$ values is implied,¹⁵ and thus $|\delta B(q)|$ and/or $\tau(q)$ are distributed. Typically, near a magnetic phase transition the correlation time becomes longer, causing $1/T_1$ to increase, a phenomenon known as critical slowing down. Below the ordering temperature, the fluctuating amplitude decreases and $1/T_1$ is reduced.

The stretched exponential form in Eq. (3) is often useful to parameterize the data because it involves only a few parameters and can be used to approximate $G_{\text{rlx}}(t)$ over a wide temperature range. However, for the materials under investigation here, we have found that for large $1/T_1$ and small K the relaxation function can often be better approximated over a limited temperature range by the sum of two exponentials:

$$G_{\text{rlx}}(t) = A_f \exp(-\lambda_f t) + A_s \exp(-\lambda_s t), \quad (4)$$

where λ_f and λ_s correspond to fast and slow local-field fluctuation rates τ^{-1} , respectively. This fitting function is for a bi-modal distribution of fluctuation rates, and its appropriateness is discussed in detail in Section III below.

B. Sample preparation

The $\text{La}_{1-x}\text{Ca}_x\text{MnO}_3$ samples studied here were polycrystalline materials prepared either as boules in an optical floating zone furnace ($0 \leq x \leq 0.18$) or as sintered powders ($0.33 \leq x \leq 1.0$). In general, polycrystalline materials of $(\text{La,Ca})\text{MnO}_3$ are more compositionally homogeneous than comparable volumes of single crystals, because of relatively less Ca evaporation and more stable growth conditions. The samples were characterized using x-ray diffraction, resistivity and susceptibility. All samples were greater than 98% single phase.

II. EXPERIMENTAL RESULTS: AN OVERVIEW

A. LaMnO_3 and CaMnO_3 : Antiferromagnets

The compounds LaMnO_3 and CaMnO_3 are the AFM end members of the $(\text{La,Ca})\text{MnO}_3$ series. They are both insulating, but do not exhibit charge ordering. LaMnO_3 possesses A-type AFM order³ below the Néel temperature $T_N \approx 139$ K, in which ferromagnetic (FM) MnO_2 sheets are antiferromagnetically aligned with one another. Conversely, CaMnO_3 possesses G-type AFM order³ below $T_N \approx 123$ K, where each Mn atom is antiferromagnetically aligned with its nearest neighbor.

Figure 1 shows the temperature dependence of the two muon frequencies observed in LaMnO_3 in zero applied field, together with their amplitudes and fractional linewidths $1/(2\pi\nu_{\mu 1}T_{2i})$. These two frequencies have the same temperature dependence, and their signal amplitudes $(A_{\text{osc}})_i$ are essentially the same and independent of temperature. Note that the fractional linewidths below T_N are very narrow (≤ 2 %), as seen in the bottom frame of Fig. 1.

Figure 2 shows the temperature dependence of the spin-lattice relaxation rate $1/T_1$ and the relaxing amplitude A_{rlx} in LaMnO_3 . These data were obtained by fitting the relaxing part of $G_z(t)$ to Eq. (3). The exponent K was found to be consistent with a simple exponential relaxation function ($K = 1$) over the entire temperature region measured. The sharp rise in $1/T_1$ at T_N and fall just below T_N indicates a very narrow range of critical temperatures for this compound. The magnitude of $1/T_1$ is temperature independent above T_N . Note also that A_{rlx} is equal to one above T_N , but falls within a few degrees to its polycrystalline average of about $1/3$ just below T_N , indicating that the transition to the AFM state is quite sharp in temperature. Both the rapid fall in A_{rlx} and the sharp rise in $1/T_1$ occur very near the temperature where the observable muon frequencies approach zero. The latter is shown in the bottom frame of Fig. 2, where the two muon frequencies have been normalized at 120 K to show that they have the same temperature dependence. Finally, the top frame of Fig. 2 shows that a rather modest field of 3 kOe applied parallel to the muon spin polarization destroys the sharp critical behavior in $1/T_1$.

Figures 3 and 4 show comparable data for CaMnO_3 . In this compound three muon frequencies are observed at low temperatures, but only the lowest frequency line $\nu_{\mu 1}$ is clearly observable at temperatures above about 90 K. The magnitude of $\nu_{\mu 1}$ approaches zero frequency near T_N , as seen in the middle frame of Fig. 3 and the bottom frame of Fig. 4. The relative linewidths $1/(2\pi\nu_{\mu i}T_{2i})$ are somewhat broader in CaMnO_3 than in LaMnO_3 . The dynamical signal in CaMnO_3 is shown in the top two frames of Fig. 4, and exhibits a behavior similar to that in LaMnO_3 ; e.g., a very narrow critical region, as indicated by sharp transitions in $1/T_1$ and A_{rlx} , and a temperature-independent $1/T_1$ behavior above T_N .

Summarizing our results on the two end compounds, LaMnO_3 and CaMnO_3 exhibit sharp transitions into their magnetically ordered states, and their dynamic relaxation functions $G_{\text{rlx}}(t)$ can be described by a single exponentially decaying time dependence.

B. $\text{La}_{0.94}\text{Ca}_{0.06}\text{MnO}_3$: Insulating Canted Antiferromagnet

As Ca is substituted for La one introduces chemical disorder into the lattice and holes into the Mn^{3+} electronic structure, producing Mn^{4+} . An additional consequence is that the local JT distortions are reduced as the holes become more abundant, because Mn^{4+} is not a JT-active ion. In $\text{La}_{0.94}\text{Ca}_{0.06}\text{MnO}_3$, for example, the AFM order found in LaMnO_3 begins to show traces of FM, although only through a canting of the Mn spin moments.³ The system remains insulating, although its resistivity drops in magnitude compared to the undoped LaMnO_3 (Fig. 5).

The μSR data for this system are now discussed. First, no oscillating component was observed. This is likely due to a complicated magnetic structure which washes out observation of a discreet muon frequency or frequencies. The μSR data for the relaxing component G_{rlx} in $\text{La}_{0.94}\text{Ca}_{0.06}\text{MnO}_3$ are shown in Fig. 6. These data were obtained by fitting G_{rlx} with the stretched-exponential form in Eq. (3). One sees that the amplitude A_{rlx} drops sharply and the spin-lattice relaxation rate $1/T_1$ shows a peak at $T \approx 122$ K, indicating the onset of magnetic order. Note that Ca doping has decreased the transition temperature compared to the undoped LaMnO_3 . Comparing the zero-field relaxation rates in $\text{La}_{0.94}\text{Ca}_{0.06}\text{MnO}_3$ to those in LaMnO_3 one notes that the width of the peak in $1/T_1$ is larger in the Ca-doped compound. This is so despite the fact that the transition width, as measured by the reduction in the relaxing amplitude A_{rlx} near the ordering temperature, remains quite narrow. Furthermore, the relaxation function in $\text{La}_{0.94}\text{Ca}_{0.06}\text{MnO}_3$ is no longer exponential, as it was in LaMnO_3 . This is shown in the middle frame of Fig. 6, where the temperature dependence of the exponent K in Eq. (3) is displayed. G_{rlx} actually begins to deviate from its exponential form ($K = 1$) at a temperature slightly above the peak temperature in $1/T_1$. The value of K continues to decline as the temperature is lowered below the transition. As shown here and below, this non-exponential behavior and broadening of the transition in $1/T_1$ is characteristic of the systems containing both La and Ca. Finally, as in both the undoped LaMnO_3 and CaMnO_3 compounds, the application of a small applied field tends to destroy the signature of the magnetic ordering in the spin-lattice relaxation rate (Fig. 6, bottom frame).

C. $\text{La}_{0.82}\text{Ca}_{0.18}\text{MnO}_3$: Ferromagnetic Insulator

The data in $\text{La}_{0.82}\text{Ca}_{0.18}\text{MnO}_3$, in which the level of doping is sufficient to induce ferromagnetism, is now discussed. As shown in Fig. 5, the magnitude of the resistivity in this compound is lower than that of the $\text{La}_{0.94}\text{Ca}_{0.06}\text{MnO}_3$ material, indicating that the addition of doped holes is pushing the system closer to a conducting state. The material remains insulating, however. According to the phase diagram of Cheong and Hwang⁹ this material is a FM insulator with a transition to a CO state below about 60 K. Note that the resistivity for this compound shows a marked upturn at temperatures below about 80 K (see Fig. (5)).

Figure 7 shows the temperature dependence of A_{rlx} , K and $1/T_1$ resulting from a fit to a stretched-exponential function for G_{rlx} . A sharp peak in the spin-lattice relaxation rate is evident at temperatures near 182 K, and a broader peak is evident at lower temperatures near 110 K. The sharpness of the peak at 182 K is characteristic of critical slowing down near a magnetic phase transition. This transition to an ordered state is also reflected in the sharp reduction in the magnitude of A_{rlx} below the same temperature. The peak temperature is consistent with the ferromagnetic transition temperature in the published phase diagram,⁹ indicating that $T_C = 182$ K for this material. As in the $\text{La}_{0.94}\text{Ca}_{0.06}\text{MnO}_3$ compound, the exponent K decreases at temperatures below T_C .

Figure 8 shows the temperature dependence of the measured muon frequency ν_μ , together with its fractional linewidth $1/(2\pi\nu_\mu T_2)$ from the oscillating portion of G_{rlx} . For comparison, the temperature dependence of $1/T_1$, shown in the bottom panel of the same figure, exhibits a peak where ν_μ tends to zero. Note that only a single frequency is observed, unlike in LaMnO_3 or CaMnO_3 , which display multiple muon frequencies. This indicates that the Ca doping is sufficient to have created a rather simple (FM) magnetic structure, so that a discrete muon frequency is observable, unlike the case of $\text{La}_{0.94}\text{Ca}_{0.06}\text{MnO}_3$. This observable frequency clearly corresponds to the buildup of the FM magnetization below T_C , but observation of the FM order parameter is only visible in the temperature range $150 \leq T \leq 180$ K. At the lowest temperatures where ν_μ can be observed, $T \approx 0.82T_C$, the fractional spread in frequencies ($1/(2\pi\nu_\mu T_2)$) is at least an order of magnitude larger than found in the undoped LaMnO_3 . This presumably reflects the local disorder in the material, which shows up as a spread in local magnetic fields, even though the transition temperature itself remains fairly sharp.

Below 150 K the ability to resolve a discrete muon frequency in $\text{La}_{0.82}\text{Ca}_{0.18}\text{MnO}_3$ vanishes, possibly due to an increasing linewidth or to a change in the magnetic state. At still lower temperatures, the muon relaxation rate $1/T_1$ shows a broad maximum, indicating a change in the Mn-ion spin dynamics. To observe this broad maximum it was necessary to freeze the value of K in the least-squares fitting procedure so that the form of the relaxation function would remain the same over the temperature range below about 170 K.

D. $\text{La}_{0.67}\text{Ca}_{0.33}\text{MnO}_3$: Ferromagnetic Conductor

For $\text{La}_{0.67}\text{Ca}_{0.33}\text{MnO}_3$ the Ca concentration is sufficient to produce a conducting state below the FM transition temperature $T_C \approx 270$ K (see Fig. 5). These data are from the same sample as used previously;¹⁶ however, the current data are of greater statistical precision than those previously reported and were taken at smaller temperature intervals near T_C .

Figures 9 and 10 show the parameters obtained from fitting the relaxation function $G_z(t)$ using the stretched exponential form in Eq. (3) for G_{rlx} . Only a single muon frequency ν_μ is found, the temperature dependence of which is shown in the middle frame of Fig. 9. The fractional inhomogeneous linewidth $1/(2\pi\nu_\mu T_2)$ is independent of temperature and yields about the same fractional width as in the insulating FM compound $\text{La}_{0.82}\text{Ca}_{0.18}\text{MnO}_3$. The spin-lattice relaxation rate $1/T_1$ is plotted in Fig. 10, together with the exponent K and the amplitude A_{rlx} . The latter shows that the FM transition is not as sharp in this material as in the previously discussed compounds. Furthermore, the exponent K falls dramatically below T_C , reaching values as low as about 0.2. Finally, the temperature dependence of $1/T_1$ reveals a rather broad peak, with large relaxation rates extending over a temperature range of nearly 75 K below T_C . This persistence of a sizeable relaxation rate below the magnetic ordering temperature is more prominent at this Ca concentration than at any other presented here. Finally, a small applied magnetic field of only 1 – 3 kOe destroys the peak in $1/T_1$ near T_C .

E. $\text{La}_{0.33}\text{Ca}_{0.67}\text{MnO}_3$: Charge Ordering and Antiferromagnetism

When $0.50 \leq x \leq 0.88$ in $\text{La}_{1-x}\text{Ca}_x\text{MnO}_3$ the system undergoes a CO transition, followed by AF order at lower temperatures.⁹ The highest CO transition temperature appears to occur for $x \approx 2/3$ where $T_{co} \approx 270$ K and $T_N \approx 125 - 150$ K. These numbers are determined largely from dc susceptibility and resistivity measurements.⁹ The μSR relaxation data between $5 \leq T \leq 250$ K for $\text{La}_{0.33}\text{Ca}_{0.67}\text{MnO}_3$ are shown in Fig. 11, again using a stretched exponential form for G_{rlx} . No μSR oscillations were observed in this material. The temperature dependence of the spin-lattice relaxation rate $1/T_1$ shows two peaks, one near the Néel temperature $T_N \approx 150$ K and a lower, broader peak centered around 80 K. The temperature dependence of the relaxing asymmetry A_{rlx} shows a decrease from 100% to about 33% near 150K, which is the signature of magnetic order in a polycrystalline material. This onset of magnetic order coincides with the peak in $1/T_1$, but the decrease in A_{rlx} occurs over a 20 – 30 K temperature range, which is comparable to that in $\text{La}_{0.67}\text{Ca}_{0.33}\text{MnO}_3$, but considerably larger than in the lower-doped samples discussed above. Also, similar to the observations in the previously discussed Ca-doped compounds, the exponent K decreases from about 1 above T_N to $K \leq 0.4$ below T_N .

F. Ferromagnetic Materials $\text{La}_{0.82}\text{Ca}_{0.18}\text{MnO}_3$ and $\text{La}_{0.67}\text{Ca}_{0.33}\text{MnO}_3$: A two-exponential analysis

As mentioned above, the stretched-exponential relaxation function is characterized by only a few parameters and can therefore provide a useful parameterization of the data over a broad temperature range. For example, a deviation from the expected¹⁷ and usually observed¹⁸ simple exponential form ($K = 1$) is readily detectable. However, careful examination of the data in Figs. 9 and 10 raises some concerns about the particular applicability of this function in $\text{La}_{0.67}\text{Ca}_{0.33}\text{MnO}_3$. First, the exponent K reaches a very small value just below T_C , where $K \leq 0.2$. Even in spin glasses such as AgMn , where a stretched exponential μSR relaxation function is observed, the exponent $1/3 \leq K \leq 1$.¹⁹ (In AgMn a distribution of energy barriers for Mn spin rotation yields a broad distribution of correlation

times τ .) Second, in $\text{La}_{0.67}\text{Ca}_{0.33}\text{MnO}_3$ the peak in $1/T_1$ actually occurs at a temperature *below* T_C (Figs. 9 and 10), rather than being at T_C as expected. This effect is not seen in the other materials and most likely occurs because, in the temperature region where K is rapidly changing, the $1/T_1$ values at different temperatures are not derived from the same functional form. These issues suggest that a more refined analysis may be useful.

Under ideal conditions determination of the precise shape of a decaying curve requires observation of the decay function over many decades with very high statistics.¹⁵ Although μSR data do not always meet these stringent criteria, we find that the relaxation function G_{rlx} can be better approximated by a sum of two exponentials (Eqn. 4), rather than a stretched exponential, when $K < 1$ and $1/T_1$ is reasonably large (usually $\geq 0.1\mu\text{s}^{-1}$). These conditions are realized for the two ferromagnetic materials $\text{La}_{0.82}\text{Ca}_{0.18}\text{MnO}_3$ and $\text{La}_{0.67}\text{Ca}_{0.33}\text{MnO}_3$, over a limited temperature range. This is illustrated in Fig. 12, which displays $G_{\text{rlx}}(t)$ in $\text{La}_{0.67}\text{Ca}_{0.33}\text{MnO}_3$. The top frame shows least squares fits for a simple exponential ($K = 1$) and a stretched exponential ($K = 0.63$). Clearly the stretched exponential function yields a better fit to the data. The bottom frame in this figure shows a fit to the sum of two exponentials using Eqn. 4; one can see at early times that the two-exponential fit is slightly better than that using the stretched exponential form.

To more precisely illustrate the two-exponential nature of G_{rlx} in $\text{La}_{0.67}\text{Ca}_{0.33}\text{MnO}_3$ near T_C , in Fig. 13 we plot $-t/\ln(G_{\text{rlx}})$ versus t on a log-log plot, together with the calculated curves from the fits to the stretched- and two-exponential functions shown in Fig. 12. Plotted in this way, a purely exponential relaxation function yields a horizontal line (zero slope); as the exponent K of the stretched-exponential is decreased from one, the calculated curve remains linear with slope $(1-K)$. Clearly, the two-exponential model function yields a better representation of the data. An analysis of the relaxation function in $\text{La}_{0.82}\text{Ca}_{0.18}\text{MnO}_3$ yields similar results.

As stated above, fitting a relaxing curve to the sum of two or more exponentials is not rigorously unique. Credible results are obtained for Ca concentrations $x = 0.18$ and 0.33 when $K < 1$ and $1/T_1 \geq 0.1\mu\text{s}^{-1}$, however, because the two rates λ_f and λ_s in Eq. 4 differ by more than a factor of ten. This is illustrated in Fig. 14. For $\text{La}_{0.92}\text{Ca}_{0.08}\text{MnO}_3$ and $\text{La}_{0.33}\text{Ca}_{0.67}\text{MnO}_3$, although a stretched-exponential relaxation function fits the data reasonably well, the rates $1/T_1$ were too small to yield good, convergent two-exponential fits over a temperature range wide enough to produce interpretable results.

Figs. 15 and 16 show the temperature dependence of the parameters λ_f and λ_s obtained from fitting G_{rlx} in $\text{La}_{0.82}\text{Ca}_{0.18}\text{MnO}_3$ and $\text{La}_{0.67}\text{Ca}_{0.33}\text{MnO}_3$, respectively, using Eqs. 3 and 4. The two-exponential fits could only be performed over a limited temperature range above and below T_C , where the relaxation rate $1/T_1$ is large enough, as explained above. Sufficiently far above T_C , where $K \approx 1$, the data are well represented by a single exponential function. The open symbols correspond to the temperature region where two-exponential fits were feasible. The closed symbols at higher temperatures (top frames Figures 15 and 16) are from the single exponential fits. In order that all of the plotted data for $\text{La}_{0.67}\text{Ca}_{0.33}\text{MnO}_3$ in the top frame of Fig. 16 correspond to an exponential functional form, some data near 180 K were omitted from this plot, because a two-exponential fit was not feasible and the exponent K in Eq. 3 was significantly less than 1. The temperature dependence of the parameters A_f and A_s are shown in Fig. 17. Here $A_f + A_s = A_{\text{rlx}}$.

Analyzed in this way the data for $\text{La}_{0.82}\text{Ca}_{0.18}\text{MnO}_3$ and $\text{La}_{0.67}\text{Ca}_{0.33}\text{MnO}_3$ yield very

interesting results. First we note that in both materials only λ_f shows a peak at T_C , characteristic of the slowing down of spins near their magnetic ordering temperature. The temperature dependence of λ_s shows no such peak, displaying only temperature independent behavior below T_C . Furthermore, the relaxation rates λ_f and λ_s differ by at least an order of magnitude, with $\lambda_s \approx 40\lambda_f$ below T_C . The ratio of amplitudes A_f/A_s near and below T_C is ≈ 3.0 in $\text{La}_{0.82}\text{Ca}_{0.18}\text{MnO}_3$ and ≈ 1.5 in $\text{La}_{0.67}\text{Ca}_{0.33}\text{MnO}_3$. Finally, as seen in Fig. 17, the amplitudes remain approximately independent of temperature below T_C in $\text{La}_{0.82}\text{Ca}_{0.18}\text{MnO}_3$, whereas A_f increases and A_s decreases below T_C in $\text{La}_{0.67}\text{Ca}_{0.33}\text{MnO}_3$.

III. ANALYSIS AND DISCUSSION OF RESULTS

A. Muon lattice sites

The observation of two muon frequencies below T_N in LaMnO_3 indicates that the muon occupies magnetically inequivalent sites in this material. A similar situation was observed by Holzschuh *et al.*,²⁰ who used μSR to study the muon's behavior in a series of single-crystal orthoferrite REFeO_3 ($\text{RE} = \text{rare earth}$) materials having the same crystal symmetry as the $(\text{La,A})\text{MnO}_3$ samples used in our experiments. Holzschuh *et al.* found that the muon occupies three different crystalline sites at low temperatures in both ErFeO_3 and YFeO_3 but that, due to thermal activation, only one of these sites remains stable at temperatures above 100 and 300 K, respectively. This most predominant and stable site is located about 1 \AA from the O(1) oxygen atoms (as defined below) in the REO_2 plane.

As stated earlier the observed muon frequency ν_μ is given by $(\gamma_\mu/2\pi)B$, where the local magnetic field B arises from the sum of a transferred hyperfine field B_{hyp} and a local dipolar field B_{dip} . In oxides, where the muon is bound about 1 \AA from an oxygen atom, the hyperfine field is in part due to the formation of a muon-oxygen covalent bond.²¹ Holzschuh *et al.* found that their data in the orthoferrites were consistent with $B_{hyp} \ll B_{dip}$, however. A similar finding has been reported from μSR experiments in the cuprates.²² It is therefore reasonable to assume that B_{hyp} is also negligible in the manganites.

Using the recently measured²³ orthorhombic structure of LaMnO_3 , where the Mn sit at $(0, 0.5, 0)$ and the oxygen O(1) at $(0.073, 0.485, 0.25)$ and O(2) at $(0.224, 0.304, 0.039)$, we calculated the dipole fields in the unit cell to search for possible muon sites in a locus of about 1 \AA from either the O(1) or O(2) sites. Here the atomic coordinates are given in fractions of the lattice spacings (5.542 \AA , 5.732 \AA , 7.783 \AA). The calculated dipole fields were compared to the measured low-temperature frequencies in LaMnO_3 , $\text{La}_{0.67}\text{Ca}_{0.33}\text{MnO}_3$ and CaMnO_3 . In LaMnO_3 there are two observed low-temperature frequencies, $\nu_{\mu 1} = 84.90 \text{ MHz}$ and $\nu_{\mu 2} = 128.8 \text{ MHz}$, corresponding to local magnetic fields of $1.6 \text{ kOe}/\mu_B$ and $2.4 \text{ kOe}/\mu_B$, respectively. We find two muon sites which are consistent with these data. The first site [Mu(1), at $(0.06, 0.71, 0.25)$] is about 1 \AA from O(1) and is quite close to the Holzschuh site found for the orthoferrites. The second site [Mu(2), at $(0.38, 0.34, 0.0)$] is about 1 \AA from O(2). The calculated dipole fields in LaMnO_3 (Mn spin $S = 2$) for the known AFM structure are 1.6 and $2.4 \text{ kOe}/\mu_B$ for Mu(1) and Mu(2), respectively, which are in excellent agreement with the measured values. Furthermore, these same two sites reproduce the single measured low-temperature frequency in FM $\text{La}_{0.67}\text{Ca}_{0.33}\text{MnO}_3$, $\nu_\mu = 75 \text{ MHz}$, or $1.5 \text{ kOe}/\mu_B$; i.e., the calculated value of B_{dip} is $1.5 \text{ kOe}/\mu_B$ for *both* of these sites,

using $S = 2(1-x) + 1.5x$, $x = 0.33$. Finally, in CaMnO_3 three muon frequencies are observed: $\nu_{\mu 1} = 14.3$ MHz, $\nu_{\mu 2} = 41.2$ MHz and $\nu_{\mu 3} = 86.5$ MHz, corresponding to 0.35 kOe/ μ_B , 1.01 kOe/ μ_B , and 2.13 kOe/ μ_B , respectively. The calculated dipolar fields yield $B_{dip} = 0.27$ kOe/ μ_B for Mu(2) and $B_{dip} = 2.3$ kOe/ μ_B for Mu(1) using $S = 1.5$, in good agreement with $\nu_{\mu 1}$ and $\nu_{\mu 3}$, respectively. Thus, these two muon sites are consistent with all of the measured low-temperature muon frequencies in LaMnO_3 , $\text{La}_{0.67}\text{Ca}_{0.33}\text{MnO}_3$ and CaMnO_3 except the $\nu_{\mu 2}$ frequency in CaMnO_3 , which corresponds to a metastable position, as discussed below.

A more definitive identification of the muon sites in these materials would require single crystals, in which not only the magnitude but also the direction of the local field could be determined. Nevertheless, from the measurements reported here one may strongly infer that the positive muon occupies positions within about 1 \AA of both the O(1) and O(2) oxygen atoms across the (La,Ca)MnO₃ series. Because a small amount of local lattice dilation due to the electrostatic field of the muon can reduce the calculated dipole fields by about 10%, and because we neglect the possible effects of any small transferred hyperfine fields, we estimate that our position assignments are uncertain to at least 0.2 \AA . Although knowledge of the muon site is very important for some types of experiments, we point out that the interpretation of our primary results, the Mn-ion relaxation rates, does not depend on the exact location of the muon in the lattice.

It is important to know whether the muon is stationary in the lattice, however, because rapid muon motion can mimic the relaxation of the Mn spins themselves. The occurrence of stable muon sites does not apply to CaMnO_3 , for example. Here three muon frequencies were observed, with only the lowest frequency $\nu_{\mu 1}$ persisting at temperatures as high as T_N . The amplitude corresponding to $\nu_{\mu 1}$ also increases monotonically with temperature, as seen in the top frame of Fig. 3. This is likely due to a change in the muon site population with temperature, as found in the orthoferrites.

A transfer of polarization between different muon sites occurs as a consequence of the thermal activation of the positive muon from a relatively shallow trapping site to a deeper one.²⁰ To affect the observed relative populations the muon hopping time τ_h must be sufficiently small; e.g., significant population change takes place at a temperature where $\tau_h \Delta\omega_\mu \leq 1$, with $\Delta\omega_\mu$ the frequency difference between the two sites.²⁰ While we do not attempt a detailed analysis of the muon motion in CaMnO_3 , we estimate $\tau_h \cong 0.003 \mu\text{s}$ at $T \cong 80$ K in CaMnO_3 , assuming $\Delta\omega_\mu \cong 2\pi \times 50$ MHz, corresponding to hopping between sites with frequencies $\nu_{\mu 3}$ and $\nu_{\mu 1}$, for example. We note, however, that the $1/T_1$ linewidth is independent of temperature above T_N up to 275 K. This indicates that any postulated muon hopping rate out of the most stable site in CaMnO_3 (corresponding to $\nu_{\mu 1}$) is small compared to the inverse of the Mn spin correlation time τ^{-1} . An order of magnitude estimate for τ^{-1} at high temperatures in CaMnO_3 yields $10^{11} - 10^{12} \text{ s}^{-1}$. Thus, we deduce that $3 \times 10^8 \leq \tau_h^{-1} \ll 10^{11} - 10^{12} \text{ s}^{-1}$ in CaMnO_3 for $T \geq T_N$.

Having obtained direct evidence for unstable muon sites in CaMnO_3 , one must consider the possibility of muon motion in the other compounds, particularly at the highest measured temperatures. Significant muon hopping is ruled out below 170 K in LaMnO_3 , for the following reasons. Unlike in the orthoferrites or in CaMnO_3 , the two signal amplitudes which we measure in LaMnO_3 remain temperature independent below T_N (top frame, Fig. 1). Thus these data, and the constancy of the spin-lattice relaxation rate above T_N , indicate that the muon shows no sign of occupying a metastable site below at least 170 K in LaMnO_3 .

One might inquire whether the falling of the rate λ_s in $\text{La}_{0.67}\text{Ca}_{0.33}\text{MnO}_3$ above about 267 K (Fig. 16) could be caused by muon motion. This would require a muon hopping rate $\tau_h^{-1} \gg \tau_s^{-1}$, the inverse correlation time of the ‘slow’ Mn spins. We estimate $\tau_s^{-1} \approx 2 \times 10^{11} \text{ s}^{-1}$, where τ_s^{-1} is derived from the measured $\lambda_s \approx 2 \mu\text{s}^{-1}$ and the relation $\lambda_s = 2\omega_\mu^2\tau_s$, using the low-temperature muon frequency $\omega_\mu = 2\pi \times 75 \text{ MHz}$. This yields a value for τ_h^{-1} in $\text{La}_{0.67}\text{Ca}_{0.33}\text{MnO}_3$ which exceeds the upper limit found above for the most stable site in CaMnO_3 at comparable temperatures. (This site, Mu(2), is also found in $\text{La}_{0.67}\text{Ca}_{0.33}\text{MnO}_3$.) The disorder induced by doping in $(\text{La,Ca})\text{MnO}_3$ should help to stabilize the muon position, and it therefore seems unlikely that muon motion is a significant factor in our measurements.

B. Muon precession frequencies

The temperature dependence of the ν_μ reflects the growth of the local magnetization below the ordering temperature. We have performed an analysis of the temperature dependence of the muon frequency below the ordering temperatures in those materials where the muon frequency is observable. The temperature dependence of $\nu_\mu(T)$ can be parameterized as follows:

$$\nu_\mu(T) = \nu_{\mu 0}(1 - T/T_M)^\beta \quad (5)$$

Fits were carried out in a limited temperature range near the ordering temperature T_M ($0.80T_M \lesssim T \lesssim T_M$), reflecting the limited range of validity for Eq. (5). (Strictly speaking Eq. (5) is valid only in the asymptotic critical region of a second order magnetic phase transition. Often this expression works well outside of this region, however.) The fits are shown as solid lines in the lower frames of Figures 2 and 4 for LaMnO_3 and CaMnO_3 , respectively. In LaMnO_3 the two frequencies were normalized at $T = 120 \text{ K}$; one sees from the plot in Fig. 2 that the two signals possess the same temperature dependence. We obtained $\beta = 0.340 \pm 0.008$ for LaMnO_3 and $\beta = 0.53 \pm 0.03$ for CaMnO_3 ; in the latter case only the more stable frequency $\nu_{\mu 1}$ was included in the fit. The exponent for LaMnO_3 is consistent with measured critical exponents in 3D Heisenberg antiferromagnets,²⁴ while the exponent for CaMnO_3 yields the mean field value of 1/2. The presence of muon diffusion (i.e., change in muon site population) in CaMnO_3 may render this value unreliable, however.

The fit for the $\text{La}_{0.82}\text{Ca}_{0.18}\text{MnO}_3$ material, carried out over the observable temperature range ($0.8 \lesssim T/T_C \lesssim 1.0$), is shown in the middle frame of Fig. 8. This yielded $T_C = 182.2 \pm 1.8 \text{ K}$ and $\beta = 0.49 \pm 0.09$. A fit to the $\text{La}_{0.67}\text{Ca}_{0.33}\text{MnO}_3$ data between $T = 220 - 267 \text{ K}$ yielded $T_C = 268 \pm 0.4 \text{ K}$ and $\beta = 0.233 \pm 0.013$.²⁵

In each of these cases the fitted frequency curves give a magnetic ordering temperature which is consistent with the peak in the spin-lattice relaxation rates arising from critical slowing down of the Mn spins. Note that for $\text{La}_{0.67}\text{Ca}_{0.33}\text{MnO}_3$ this is only true for the two-exponential fit, not for the stretched exponential fit. This fact is further indication that the two-exponential fit is a better representation of the data near T_C for this system.

It is not clear how to interpret the values of β obtained from the FM materials $x = 0.18$ and 0.33 , for the following reasons. The insulating $x = 0.18$ material lies close to the boundary where canted AFM is observed. Furthermore, the growth of the FM order parameter in this compound may be influenced by the change in spin dynamics found below

150 K, near where the resistivity shows its anomalous increase. Either of these facts makes comparison of β with theories of conventional phase transitions dubious. Finally, as discussed below, the transition in the $x = 0.33$ conducting material may proceed via the percolation of FM clusters arising from the presence of magnetoelastic polarons, rather than via a more conventional FM second-order phase transition. At present there is, therefore, no theory to which these exponents can be compared.

C. Spin-lattice relaxation

We first discuss the zero-field spin-lattice relaxation rates in LaMnO₃ and CaMnO₃, shown in the top frames of Figs. 2 and 4, respectively. In both LaMnO₃ and CaMnO₃ G_{rlx} is well described by a single exponential $A_{\text{rlx}} \exp(-t/T_1)$. The peak in the spin-lattice relaxation rate $1/T_1$ reflects critical slowing down near T_N , and in each material the temperature region of the critical dynamics is relatively narrow. Furthermore, the zero-field transition in both materials is quite sharp, as seen by the rapid decrease in the relaxing amplitude A_{rlx} below T_N , shown in the middle frames of Figs. 2 and 4. Note that even the relatively modest ($\mu_B H \ll k_B T_N$) field $H = 3$ kOe applied parallel to the muon spin strongly affects the critical dynamics.

Both LaMnO₃ and CaMnO₃ display temperature independent spin-lattice relaxation over an extended temperature range above T_N . This is characteristic of systems fluctuating at their exchange frequency ω_e . In this instance one has¹⁷

$$1/T_1 = \sqrt{2\pi} S(S+1) \Delta^2 / (3\hbar^2 \omega_e), \quad (6)$$

where S is the Mn atomic spin ($S = 2$ for LaMnO₃ and $S = 3/2$ for CaMnO₃) and Δ is the hyperfine coupling constant between the muon spin and the spin S . The exchange frequency is related to the exchange integral J via the expression $\hbar\omega_e = J\sqrt{2zS(S+1)}/3$, where z is the number of nearest neighbor Mn spins to a given Mn spin.

We now use Eq. (6) to estimate the exchange frequency for LaMnO₃ and CaMnO₃. To do so one may obtain Δ from the value of the low temperature muon frequency ($2\pi\nu_\mu = \omega_\mu$) or frequencies. If there is a single frequency then $\Delta = \hbar\omega_\mu/S$. When there is more than one muon frequency the relaxation function takes the form $G_{\text{rlx}} = \sum_i (A_{\text{rlx}})_i \exp(-t/T_{1i})$, where the index i runs from 1 to 3 in CaMnO₃, for example. In principle, this implies that one should observe a multi-component or stretched-exponential relaxation function, which is in contradiction to the single-exponential function observed in both LaMnO₃ and CaMnO₃. However, if the individual relaxation times T_{1i} are all long compared to the characteristic time of the experiment (of the order of the muon lifetime), then

$$G_{\text{rlx}} = \sum_i (A_{\text{rlx}})_i \exp(-t/T_{1i}) \approx A_{\text{rlx}} \exp(-t/\overline{T_1}), \quad (7)$$

where $1/\overline{T_1} = \sum_i (A_{\text{rlx}})_i T_{1i}^{-1} / A_{\text{rlx}}$. In this limit a single exponential relaxation function is recovered, with a relaxation rate which is an appropriately weighted sum of rates $1/T_{1i}$. The observed relaxation times T_1 in both LaMnO₃ and CaMnO₃ are relatively long ($\approx 10-20\mu\text{s}$), and thus the individual relaxation times T_{1i} are also presumably long. This then explains the observation of an exponential relaxation function in each case.

In the motional narrowing limit,¹⁷ appropriate for relaxation above T_N , $1/T_{1i} = 2\omega_{\mu i}^2\tau_i$, so that $\Delta^2 \approx \sum_i (A_{\text{rlx}})_i (\hbar\omega_{\mu i}/S)^2/A_{\text{rlx}}$. Here τ is the Mn-ion correlation time. In LaMnO_3 the observed low temperature frequencies are $\omega_{\mu 1} = 2\pi \times 84.9$ MHz and $\omega_{\mu 2} = 2\pi \times 128.8$ MHz. These values yield an exchange frequency $\omega_e = 6.33$ THz, corresponding to an exchange integral $J = 0.85$ meV. Using the mean field expression¹⁷ $T_N = JzS(S+1)/3$ one obtains $T_N = 119$ K, in good agreement with the measured Neél temperature of 139 K. The situation is not so sanguine in CaMnO_3 , however. Here the low temperature frequencies are $\omega_{\mu 1} = 2\pi \times 14.3$ MHz, $\omega_{\mu 2} = 2\pi \times 41.2$ MHz and $\omega_{\mu 3} = 2\pi \times 86.5$ MHz, yielding $\omega_e = 2.8$ THz, $J = 0.47$ meV and $T_N = 42$ K, lower by a factor of about 3 than the measured T_N . However, if one uses *only* the lowest frequency $\nu_{\mu 1}$ for CaMnO_3 (corresponding to the ‘stable’ muon site), one obtains $\omega_e = 0.10$ THz, $J = 0.017$ meV and $T_N = 1.5$ K, an unacceptably low value even given the crudeness of the approximations used. This seems to be an indication that in CaMnO_3 muon motion makes determination of the effective coupling constant Δ ambiguous. Alternatively, the mean field approximations used to estimate T_N may not be valid in CaMnO_3 , despite the finding of a mean-field exponent for the temperature dependence of the lowest μ SR frequency $\nu_{\mu 1}$.

As the amount of Ca doping increases from zero in $\text{La}_{1-x}\text{Ca}_x\text{MnO}_3$ the width of the peak in $1/T_1$ near the magnetic transition grows larger. This is seen already for $x = 0.06$ (Fig. 6), where the width in $1/T_1$ extends over a considerably larger temperature region than does the fall in the relaxing amplitude A_{rlx} . Recall that a reduction in A_{rlx} signals the onset of magnetic order, even though no muon frequencies were observed in this material. The changing value of the exponent K also extends over a wide temperature regime around T_N , indicating that the spin dynamics are becoming inhomogeneous near T_N . This trend, a general decline in the value of K at the magnetic ordering temperature, is seen in all of the Ca-doped samples except the end compound CaMnO_3 , in which simple exponential relaxation is observed at all temperatures. Furthermore, the $1/T_1$ relaxation rates in the $x = 0.06$ and $x = 0.33$ materials tend to remain relatively large at temperatures significantly below their magnetic ordering temperatures, indicating that there is an anomalously slow (large τ) relaxation process which persists in the ordered state. Values of $K \ll 1$, combined with the real-space nature of the muon probe, suggest that the relaxation rates are therefore spatially distributed, as discussed in more detail below.

The FM $x = 0.18$ compound and the AFM $x = 0.67$ compound each exhibit an uncharacteristic increase in their spin-lattice relaxation rates well below their ordering temperatures. This change is marked by a broad maximum near $T \approx 110$ K for $x = 0.18$ ($T_C = 182$ K) and $T \approx 85$ K for $x = 0.67$ ($T_N \simeq 150$ K). It is tempting to attribute the loss of the oscillating component and the gentle rise in the relaxation rates near 110 K in $\text{La}_{0.82}\text{Ca}_{0.18}\text{MnO}_3$ to the influence of ‘charge ordering’ (CO) reported by others⁹ at $T \approx 70$ K. It is known, for example, that the dynamical spin correlations in $(\text{Bi,Ca})\text{MnO}_3$ change from ferromagnetic above the CO temperature T_{co} to antiferromagnetic below T_{co} .²⁶ We note, however, that CO observed in $\text{La}_{0.33}\text{Ca}_{0.67}\text{MnO}_3$ occurs at temperatures *above* T_N , as opposed to *below* T_C in $\text{La}_{0.82}\text{Ca}_{0.18}\text{MnO}_3$. Because μ SR cannot determine the type of magnetic correlations present in these materials (in general, this requires a momentum-dependent probe), we cannot definitively explain the change in spin dynamics below the ordering temperatures of the $x = 0.18$ and $x = 0.67$ materials. We do note the possible correlation with CO in both, however. This could be the subject of further investigation by neutron scattering, for

example.

The two FM materials under study, $\text{La}_{0.82}\text{Ca}_{0.18}\text{MnO}_3$ and $\text{La}_{0.67}\text{Ca}_{0.33}\text{MnO}_3$, exhibit a bi-modal distribution of fluctuation rates in perhaps the most interesting part of the phase diagram. The two-exponential fits to G_{rlx} [Eq. (4)] yielded relaxation rates and relative amplitudes λ_f , λ_s , A_f and A_s . We have labeled these quantities ‘f’ and ‘s’ to indicate ‘fast’ and ‘slow’ Mn-ion fluctuation rates τ^{-1} because, in general, the local muon relaxation rate $\lambda \propto \gamma_\mu^2 \sum_q |\delta B(q)|^2 \tau(q)$, as mentioned in Section IA. Here $|\delta B(q)|$ is the amplitude of the local fluctuating field and $\tau(q)$ is the Mn-ion correlation time. The relaxation rates λ_f and λ_s display very different magnitudes (Figs. 15 - 16): in each material $\lambda_s \approx 10 - 40 \times \lambda_f$. Using the relation $\lambda = 2\omega_\mu\tau$, one may derive Mn correlation times for $\text{La}_{0.67}\text{Ca}_{0.33}\text{MnO}_3$ at $T = 250$ K, for example. One obtains $\tau_f \simeq 10^{-13}$ s and $\tau_s = 5 \times 10^{-12}$ s, assuming that ω_μ at the lowest temperatures is representative of the μ^+ -Mn coupling for both the slow and fast components. It is noteworthy that only λ_f shows evidence of ‘critical slowing down’ at T_C . In the FM conductor $\text{La}_{0.67}\text{Ca}_{0.33}\text{MnO}_3$, A_f increases below T_C (and A_s decreases), while in the insulating material $\text{La}_{0.82}\text{Ca}_{0.18}\text{MnO}_3$ the fast and slow amplitudes are relatively temperature independent below T_C (Fig. 17). At T_C , A_f is also a somewhat larger in $\text{La}_{0.82}\text{Ca}_{0.18}\text{MnO}_3$ than in $\text{La}_{0.67}\text{Ca}_{0.33}\text{MnO}_3$.

This analysis is consistent with two different spatially distinguishable regions in the sample, characterized in our measurements by very different relaxation rates and temperature-dependent volumes. More specifically, although the λ_f component may exist throughout the sample volume, the λ_s component can only exist in spatially separated regions; otherwise only the slow Mn fluctuation rate (which creates the largest μSR rate and corresponds to λ_s) would be observed. The muon samples these separate regions locally through its relatively short-ranged dipolar coupling to the Mn spins (matrix element $\sim r^{-6}$). It is important to note that neither μSR relaxation component corresponds to pure LaMnO_3 or CaMnO_3 , whose relaxation rates are independent of temperature above 140 K with magnitudes $\approx 0.10 - 0.05 \mu\text{s}^{-1}$, as discussed earlier. This argues against large-scale separation of Mn^{3+} and Mn^{4+} ions. Furthermore, we note that because of the large spin wave stiffness constant observed¹⁴ near T_C in these FM materials the muon spin is not significantly relaxed by spin waves, as pointed out¹⁶ previously. Thus, these FM materials possess at least three types of fluctuations, the FM spin waves observed in neutron scattering, and the excitations associated with the λ_f and λ_s relaxation rates reported here.

We postulate that the two relaxation components observed here constitute the spin signature of magnetoelastic polarons as the system becomes FM. As discussed in the introduction to this paper, these polarons are thought to be formed from FM polarized Mn spins which surround a region of local lattice distortion, and presumably originate from the combined DE and JT interactions. These polaronic effects, together with the random replacement of La atoms by Ca, produce considerable disorder. Our measured λ_f component shows a peak in the relaxation rate at T_C , and we associate this relaxation with *overdamped* spin waves, characteristic of a disordered FM. That is, the damping of the spin waves in this scenario would be caused by a loss of translational symmetry arising from inherent disorder.

As mentioned in the introduction, a broad peak in the neutron scattering intensity centered around zero energy transfer has been observed in FM $\text{La}_{0.67}\text{Ca}_{0.33}\text{MnO}_3$.¹⁴ This peak coexists with Mn spin waves near T_C , and persists to temperatures as low as $T/T_C = 0.7$, consistent with the finite μSR rate we measure in $\text{La}_{0.67}\text{Ca}_{0.33}\text{MnO}_3$ below T_C . The neutron

linewidth Γ obeys a diffusive relaxation law, $\Gamma = Dq^2$, where $D \approx 30 \text{ meV } \text{\AA}^2$. The length scale for this diffusion was found to be 12 \AA from small angle scattering.¹⁴ We can compare this linewidth Γ with λ_f using the relation¹⁷

$$\lambda_f = 2\omega_\mu^{-2} \int \langle \mathbf{S}(q, t) \cdot \mathbf{S}(-q, 0) \rangle \exp(i\omega t) dt. \quad (8)$$

Here $\langle \mathbf{S}(q, t) \cdot \mathbf{S}(-q, 0) \rangle$ is the transverse spin-spin correlation function given by

$$\langle \mathbf{S}(q, t) \cdot \mathbf{S}(-q, 0) \rangle = k_B T \chi(q) \exp(-Dq^2 t) / (g\mu_b)^2, \quad (9)$$

where $\chi(q)$ is the static q -dependent susceptibility, k_B is Boltzman's constant and μ_B is the Bohr magneton. We take an Ornstein-Zernike form for $\chi(q)$, given by²⁸

$$\chi(q) = (g\mu_b)^2 S(S+1) / (3k_B T (q^2 + \xi^{-2}) r_1^2), \quad (10)$$

where $r_1^2 = a^2/6$ for a cubic lattice with lattice constant a , and ξ is the coherence length for the diffusive spin correlations. Evaluating these expressions for $\xi = 12 \text{ \AA}$ yields $\lambda_f = 0.18 \mu\text{s}^{-1}$, in excellent agreement with our μSR measurements of λ_f at $T = T_C$ (see Fig. 16). Thus, we associate our observed λ_f with the diffusive relaxation mode observed in quasi-elastic neutron scattering, and attribute the relaxation to *overdamped* spin waves.

The existence of overdamped FM spin waves is naturally associated with a relatively high level of charge mobility because the FM in these CMR compounds is induced by the hopping of holes via the DE interaction. By contrast, the λ_s component corresponds to a rather long correlation time of $\approx 10^{-11}$ s. This order-of-magnitude is probably inconsistent with electronic relaxation of single Mn^{3+} or Mn^{4+} spins. Other possible mechanisms might include phonon induced spin relaxation (via magnetoelastic coupling) or the slow overturning of spins associated with local polaron hopping in regions of the sample where spin and charge motion are frustrated by more extreme local lattice distortions, that is, regions which are relatively *insulating*.

The possibility that the λ_s component is associated with relatively insulating regions of the sample, while the λ_f component is associated with relatively conducting regions, is qualitatively consistent with the temperature dependence of the volume fractions A_s and A_f in the two FM materials. In the FM conductor $\text{La}_{0.67}\text{Ca}_{0.33}\text{MnO}_3$ the magnitude of A_f increases (and A_s decreases) as the temperature is lowered below T_C and the material becomes more conducting. By contrast, in the insulating FM $\text{La}_{0.82}\text{Ca}_{0.18}\text{MnO}_3$ the volume fractions A_f and A_s are independent of temperature. This suggests that even significantly below T_C in conducting $\text{La}_{0.67}\text{Ca}_{0.33}\text{MnO}_3$ there exist relatively non-conducting regions which are the remnants of the inhomogeneity produced by isolated polarons existing above T_C in these materials. These less conducting regions could be caused by an uneven distribution of Ca atoms, or by more extreme local lattice distortions which inhibit charge motion. As the temperature is lowered below T_C in $\text{La}_{0.67}\text{Ca}_{0.33}\text{MnO}_3$ these less conducting regions are gradually absorbed into the larger conducting matrix of the material. This apparently does not occur in the insulating FM $\text{La}_{0.82}\text{Ca}_{0.18}\text{MnO}_3$, however, where the volume fractions are frozen below T_C .

Such a postulated scenario is consistent with our measurements, and with charge transport and structural measurements, as follows. In the two-fluid model of the resistivity²⁷

growth of the conducting charge fraction in $\text{La}_{0.67}\text{Ca}_{0.33}\text{MnO}_3$ occurs rapidly as the magnetization grows, reaching essentially 100 % just below T_C . This does not contradict the above picture from the μSR data (in which slowly fluctuating spins in relatively less metallic regions persist far below T_C) because when a conducting path is reached (at T_C) the resistivity is shorted out, even though a considerable volume fraction may still be relatively non-conducting. Thus the two-fluid model of the resistivity is similar to the picture presented here, with this one exception. The persistence of an inhomogeneous ground state below T_C is reinforced by local probes of the lattice structure,^{11,12} which are consistent with the *gradual* loss of structural inhomogeneity below T_C , similar to that reflected in the spin-lattice relaxation rates reported here in the conducting FM $\text{La}_{0.67}\text{Ca}_{0.33}\text{MnO}_3$.

IV. SUMMARY

In this paper we present μSR data for a series of (La,Ca) MnO_3 compounds, spanning the range from the AFMs LaMnO_3 and CaMnO_3 , to the FMs $\text{La}_{0.82}\text{Ca}_{0.18}\text{MnO}_3$ and $\text{La}_{0.67}\text{Ca}_{0.33}\text{MnO}_3$, to the charge-ordered material $\text{La}_{0.33}\text{Ca}_{0.67}\text{MnO}_3$. The μSR technique allows one to obtain the temperature dependence of both the local static magnetic order parameters and the Mn spin-lattice-relaxation rates τ^{-1} , where generally $10^{-4} \leq \tau^{-1} < 10^{-13} \text{ s}^{-1}$. These measurements, therefore, provide a necessary complement to other spin probes, such as neutron scattering and nuclear magnetic resonance.

From the magnitude of the measured local magnetic fields we have identified two plausible stable muon sites near the O(1) and O(2) atoms in these materials. Except for CaMnO_3 , where evidence for metastable muon sites is found, we conclude that rapid muon diffusion is not a factor in our measurements of the Mn spin dynamics. We find that the spin dynamics near the AFM and FM magnetic ordering temperatures of these compounds is quite sensitive to small applied magnetic fields, however. This may be a consequence of the FM double-exchange interaction, which is enhanced by the application of a uniform field. From the magnitude of the zero-field μSR rate above T_N in the AFM insulating parent compound LaMnO_3 we derive an exchange integral $J = 0.83 \text{ meV}$, which is consistent with the mean field expression for T_N . Our principal finding is that the addition of Ca to LaMnO_3 (or La to CaMnO_3) results in an inhomogeneous spectrum of zero-field μSR rates below the magnetic ordering temperatures in these materials. In the FM compounds $\text{La}_{0.82}\text{Ca}_{0.18}\text{MnO}_3$ and $\text{La}_{0.67}\text{Ca}_{0.33}\text{MnO}_3$ we are able to resolve this inhomogeneity into a bi-modal distribution of ‘fast’ and ‘slow’ μSR rates, corresponding to Mn spin fluctuation rates which differ by about a factor of at least 30. Because μSR is a local probe this implies that the ‘slow’ Mn fluctuations must exist in distinct spatial regions of the sample. A physical picture is hypothesized for these FM phases in which the fast Mn rates are due to overdamped spin waves characteristic of a disordered FM, and the slower Mn relaxation rates derive from distinct, relatively insulating regions in the sample. These results present direct evidence for microscopic inhomogeneity in the spin channel of the FM manganites, suggesting that a proper description of these materials probably includes more than just the simple JT and DE interactions.

This work was supported in part by the U.S. National Science Foundation, Grants DMR-9731361 (Riverside), and DMR-9510454 (Columbia), by the Japanese agency NEDO (Columbia), and the Netherlands agencies FOM and NWO (Leiden). The research was car-

ried out in part under the auspices of the U.S. DOE (Los Alamos). This work was supported by the Director for Energy Research, Office of Basic Energy Sciences.

REFERENCES

- ¹ *The Physics of Manganites*, edited by T. A. Kaplan and S. D. Mahanti (Kluwer Academic/Plenum Publishers, New York, 1999).
- ² G. H. Jonker and J. H. van Santen, *Physics* **16**, 337 (1950).
- ³ E. O. Wollen and W. C. Koehler, *Phys. Rev.* **100**, 548 (1955).
- ⁴ C. Zener, *Phys. Rev.* **82**, 403 (1951); P. W. Anderson and H. Hasegawa, *Phys. Rev.* **100**, 675 (1955); P. G. deGennes, *Phys. Rev.* **118**, 141 (1960).
- ⁵ See articles in *Colossal Magnetoresistance Oxides*, edited by Y. Tokura (Gordon and Breach, Monographs in Condensed Matter Science), to be published.
- ⁶ A. J. Millis, P. B. Littlewood, and B. I. Shraiman, *Phys. Rev. Lett.* **74**, 5144 (1995); *Phys. Rev.* **54**, 5389 (1996); **54**, 5405 (1996); H. Röder, Jun Zang, and A. R. Bishop, *Phys. Rev. Lett.* **76**, 1356 (1996).
- ⁷ H. Y. Hwang, S-W. Cheong, P. G. Radaelli, M. Marezio and B. Batlogg, *Phys. Rev. Lett.* **75** 914 (1995).
- ⁸ A. Schenck, *Muon Spin Rotation Spectroscopy: Principles and Applications to Solid State Physics* (Hilger, Bristol, 1985).
- ⁹ Sang-Wook Cheong and Harold Y. Hwang, in *Colossal Magnetoresistance Oxides*, edited by Y. Tokura (Gordon and Breach, Monographs in Condensed Matter Science), to be published.
- ¹⁰ M. F. Hundley, M. Hawley, R. H. Heffner, Q. X. Jia., J. J. Neumeier, J. Tesmer, J. D. Thompson and X. D. Wu, *Appl. Phys. Lett.* **67**, 860 (1995); M. Jaime, H. T. Hardner, M. B. Salamon, M. Rubinstein, P. Dorsey and D. Emin, *Phys. Rev. Lett.* **78**, 951 (1997).
- ¹¹ Despina Louca, T. Egami, E. L. Brosha, H. Röder, and A. R. Bishop *Phys. Rev. B* **56**, R8475 (1997); S. J. L. Billinge, R. G. DiFrancesco, G. H. Kwei, J. J. Neumeier, and J. D. Thompson, *Phys. Rev. Lett.* **77**, 715 (1996).
- ¹² C. H. Booth, F. Bridges, G. H. Kwei, J. M. Lawrence, A. L. Cornelius and J. J. Neumeier, *Phys. Rev. Lett.* **80**, 853 (1998); A. Lanzara, N. L. Saini, M. Brunelli, F. Natali, and A. Bianconi, *Phys. Rev. Lett.* **81**, 878 (1998).
- ¹³ J. A. Fernandez-Baca, P. Dai, H. Y. Hwang, C. Kloc and S-W. Cheong, *Phys. Rev. Lett.* **80**, 4012 (1998); H. Y. Hwang, P. Dai, S-W. Cheong, G. Aeppli, D. A. Tennant and H. A. Mook, *Phys. Rev. Lett.* **80**, 1316 (1998); T. G. Perring, G. Aeppli, S. M. Hayden, S. A. Carter, J. P. Remeika and S-W. Cheong, *Phys. Rev. Lett.* **77**, 711 (1996).
- ¹⁴ J. W. Lynn, R. W. Erwin, J. A. Borchers, Q. Huang, A. Santoro, J-L. Peng and Z. Y. Li, *Phys. Rev. Lett.* **76**, 4046 (1996); L. Vasiliu-Doloc, J. W. Lynn, A. H. Moudden, A. M. de Leon-Guevara and A. Revcolevschi, *J. Appl. Phys.* **81**, 5491 (1997).
- ¹⁵ Andrei A. Istratov and Oleg F. Vyvenko, *Rev. Sci. Instr.* **70**, 1233 (1999).
- ¹⁶ R. H. Heffner, L. P. Le, M. F. Hundley, J. J. Neumeier, G. M. Luke, K. Kojima, B. Nachumi, Y. J. Uemura, D. E. MacLaughlin and S-W. Cheong, *Phys. Rev. Lett.* **77**, 1869 (1996).
- ¹⁷ E. A. Turov and M. P. Petrov, *Nuclear Magnetic Resonance in Ferro- and Antiferromagnets* Halsted Press, a division of John Wiley & Sons (New York, 1972) p. 86; T. Moriya, *Prog. Theor. Phys.* **16**, 23 (1956); *ibid.* p. 641.
- ¹⁸ P. C. M. Gubbens, A. A. Moolenaar, P. Dalmas de Réotier, A. Yaouanc, F. Kayzel, J. J. M. Franse, K. Prokes, C. E. Snel, P. Bonville, J. A. Hodges, P. Imbert and P. Pari, *Hyperfine Interact. (Switzerland)* **85**, 239 (1994).

- ¹⁹ Amit Keren, Philippe Mendels, Ian A. Campbell and James Lord, Phys. Rev. Lett. **77**, 1386 (1996).
- ²⁰ E. Holzschuh, A. B. Denison, W. Kündig, P. F. Meier and B. D. Patterson, Phys. Rev. B **27**, 5294 (1983).
- ²¹ C. Boekema, Hyperfine Interact. (Switzerland) **17-19**, 305 (1984).
- ²² M. Weber, P. Birrer, F. N. Gygax, B. Hitti, E. Lippelt, H. Maletta and A. Schenck, Hyperfine Interact. **63**, 207 (1990).
- ²³ Th. Proffen, R. G. DiFrancesco, S. J. L. Billinge, E. L. Brosha and G. H. Kwei, Phys. Rev. **B60**, 9973 (1999).
- ²⁴ Sheng-Keng Ma, *Modern Theory of Critical Phenomena* (Benjamin, New York, 1976).
- ²⁵ Note that if the $x = 0.33$ data is fit over the entire temperature range ($T = 10 - 267$ K) one obtains $T_C = 272 \pm 2$ K and $\beta = 0.32 \pm 0.02$, in agreement with previously published results¹⁶.
- ²⁶ Wei Bao, J. D. Axe, C. H. Chen and S-W. Cheong, Phys. Rev. Lett. **78**, 543 (1997).
- ²⁷ M. Jaime, P. Lin, S. H. Chun, M. B. Salamon, P. Dorsey and M. Rubinstein, Phys. Rev. B **60**, 1028 (1999).
- ²⁸ Stephen W. Lovesey *Theory of Neutron Scattering from Condensed Matter* Vol. 2, Chapter 13 (Clarendon Press, Oxford, 1984).

FIG. 1. Temperature dependence of the μ SR oscillating amplitude (top), precession frequencies (middle) and fractional linewidth (bottom) in LaMnO_3 from fitting to Eq. (2).

FIG. 2. Temperature dependence of the μ SR spin-lattice relaxation rate (top), relaxing amplitude (middle) and muon precession frequencies $\nu_{\mu 1}$ and $\nu_{\mu 2}$ (bottom) in LaMnO_3 . $\nu_{\mu 2}$ has been normalized to $\nu_{\mu 1}$ at 120 K. The solid curve in the bottom frame is from a fit of the precession frequencies to Eq. (5).

FIG. 3. Temperature dependence of the μ SR oscillating amplitude (top), precession frequencies (middle) and fractional linewidth (bottom) in CaMnO_3 from fitting to Eq. (2).

FIG. 4. Temperature dependence of the μ SR spin-lattice relaxation rate (top), relaxing amplitude (middle) and muon precession frequency $\nu_{\mu 1}$ (bottom) in CaMnO_3 . The solid curve in the bottom frame is from a fit of $\nu_{\mu 1}$ to Eq. (5).

FIG. 5. Temperature dependence of the resistivity for $\text{La}_{1-x}\text{Ca}_x\text{MnO}_3$, $x = 0.0, 0.06, 0.18$ and 0.33 . Comparable data for the $x = 0.67$ sample are given in S-W. Cheong and C. H. Chen, *Colossal Magnetoresistance and Related Properties*, ed. B. Raveau and C. N. R. Rao (World Scientific), to be published.

FIG. 6. Temperature dependence of the μ SR relaxing amplitude (top), exponent (middle) and spin-lattice relaxation rate (bottom) in $\text{La}_{0.94}\text{Ca}_{0.06}\text{MnO}_3$ obtained from a fit to Eq. (3). The filled symbols are for zero applied field, and the open circles for an applied field of 2.5 kOe.

FIG. 7. Temperature dependence of the μ SR relaxing amplitude (top), exponent (middle) and spin-lattice relaxation rate (bottom) in $\text{La}_{0.82}\text{Ca}_{0.18}\text{MnO}_3$ obtained from a fit to Eq. (3).

FIG. 8. Temperature dependence of the μ SR fractional linewidth (top), precession frequency (middle) and spin-lattice relaxation rate (bottom) in $\text{La}_{0.82}\text{Ca}_{0.18}\text{MnO}_3$. The data in the top and middle frames are from a fit to Eq. (2). The solid line in the middle frame is from a fit of ν_{μ} to Eq. (5).

FIG. 9. Temperature dependence of the μ SR fractional linewidth (top), precession frequency (middle) and spin-lattice relaxation rate (bottom) in $\text{La}_{0.67}\text{Ca}_{0.33}\text{MnO}_3$ obtained from a fit to Eq. (3). The inset in the middle frame shows a fit of ν_{μ} to Eq. (5).

FIG. 10. Temperature dependence of the μ SR relaxing amplitude (top), spin-lattice relaxation rate (middle) and exponent (bottom) for zero applied field (filled symbols) in $\text{La}_{0.67}\text{Ca}_{0.33}\text{MnO}_3$ obtained from fits to Eq. (3). The open symbols in the middle frame show data in applied magnetic fields of 1 kOe and 3 kOe.

FIG. 11. Temperature dependence of the μ SR relaxing amplitude (top), spin-lattice relaxation rate (middle) and exponent (bottom) for zero applied field in $\text{La}_{0.33}\text{Ca}_{0.67}\text{MnO}_3$ obtained from fits to Eq. (3).

FIG. 12. (a) μ SR relaxation function $G_{\text{rlx}}(t)$ at $T = 270$ K. The curves show best fits using stretched exponential from Eq. (3) [$1/T_1 = 0.219(7) \mu\text{s}^{-1}$, $K = 0.63(3)$] and exponential ($K = 1$) functions. (b) A two-exponential least squares fit using Eq. (4), with $A_f = 0.60(5)$, $A_s = 0.40(5)$, $\lambda_f = 0.106(5) \mu\text{s}^{-1}$ and $\lambda_s = 0.93(11) \mu\text{s}^{-1}$.

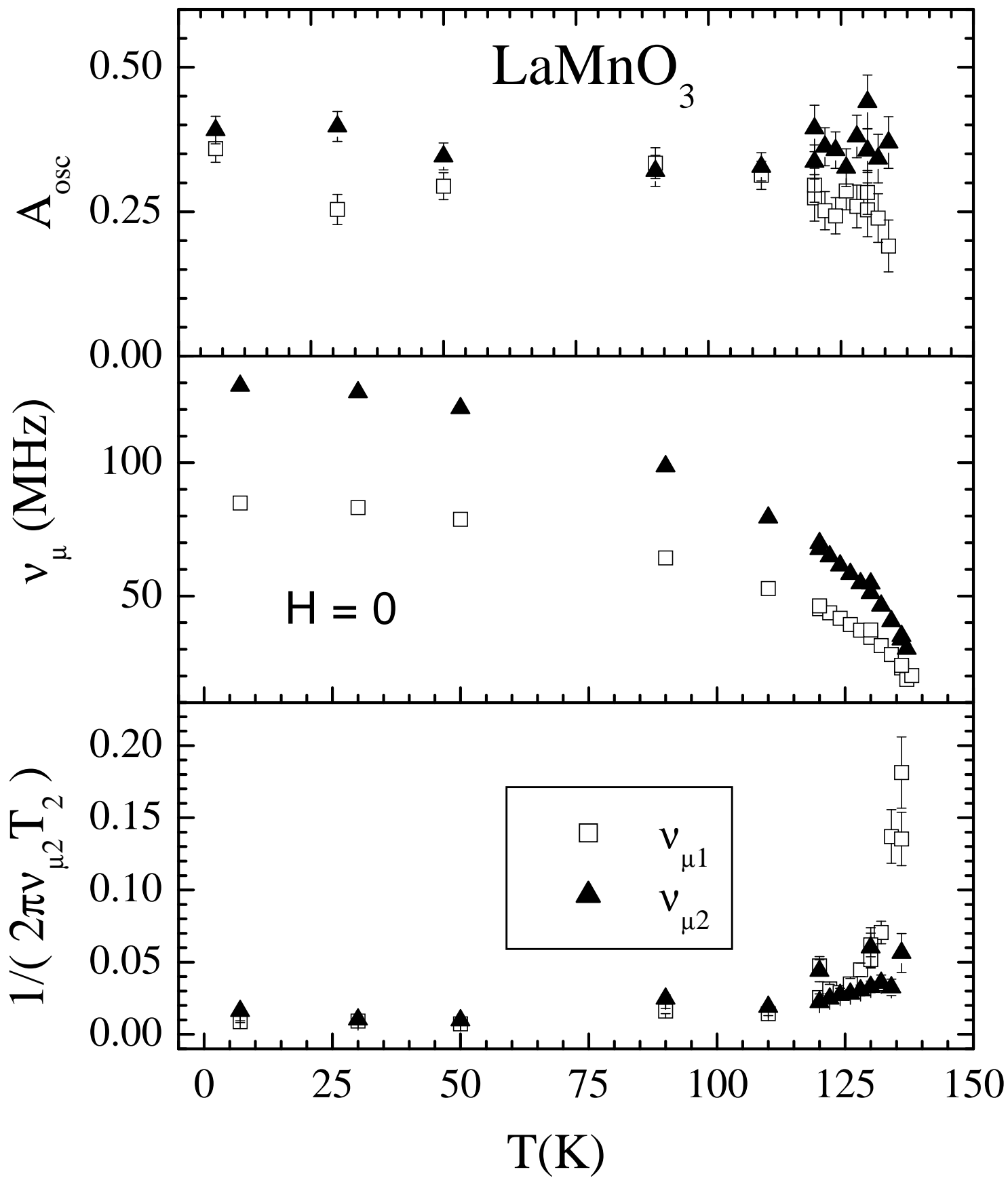
FIG. 13. The measured μ SR relaxation function $G_{\text{rlx}}(t)$ at $T = 270$ K (open squares), normalized such that $G_{\text{rlx}}(0) = 1$. The lines show calculated stretched-exponential (lower dotted line) and two-exponential (upper dashed line) functions using the fit parameters obtained from the fits shown in Figure 12. A stretched exponential $A_{\text{rlx}} \exp(-t/T_1)^K$ is linear with slope $(1 - K)$ on a plot of this type.

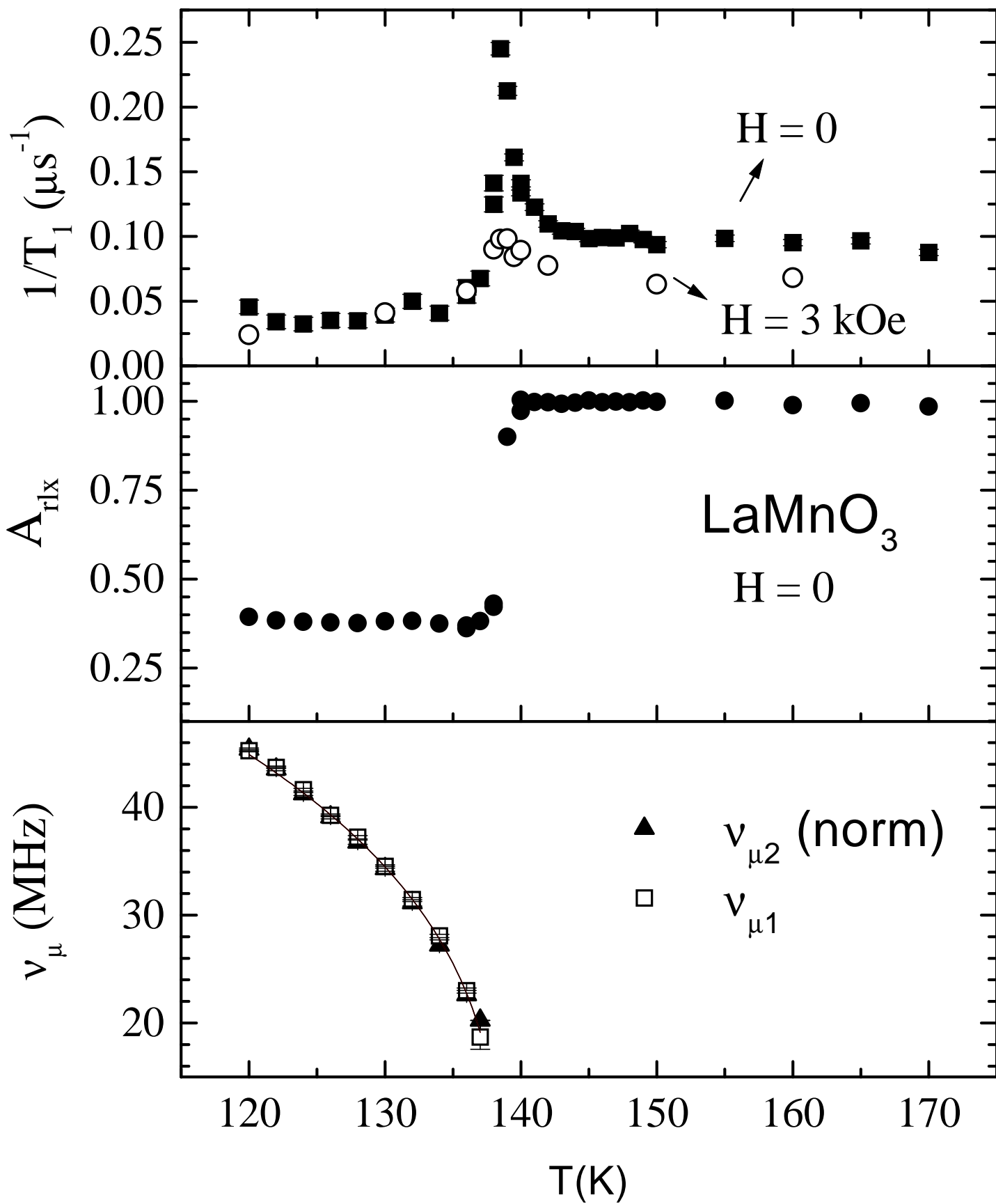
FIG. 14. Time dependence of the μ SR relaxing asymmetry G_{rlx} (open squares) for zero applied field in $\text{La}_{0.67}\text{Ca}_{0.33}\text{MnO}_3$ showing the curves λ_f (slowly relaxing curve corresponding to faster Mn spins) and λ_s (rapidly relaxing curve corresponding to more slowly relaxing Mn spins) for a two exponential fit. The curve for λ_s has been offset from the data for clarity.

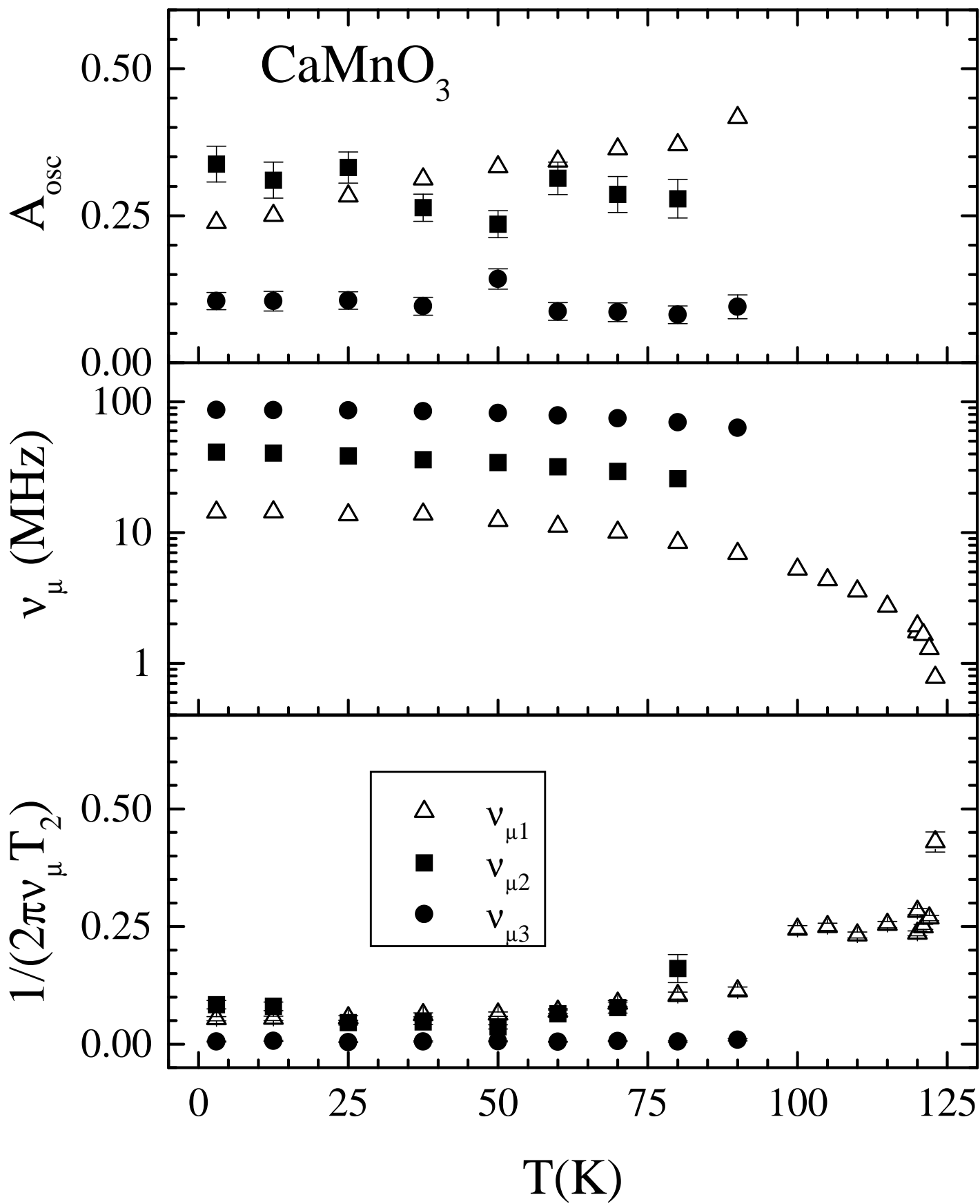
FIG. 15. Temperature dependence of the μ SR fast (λ_f , top) and slow (λ_s , bottom) spin-lattice relaxation rates for zero applied field in $\text{La}_{0.82}\text{Ca}_{0.18}\text{MnO}_3$ obtained from a fit to Eq. (3) [closed symbols, exponent $K \simeq 1$ in Eq. (3)] and Eq. (4) [open symbols].

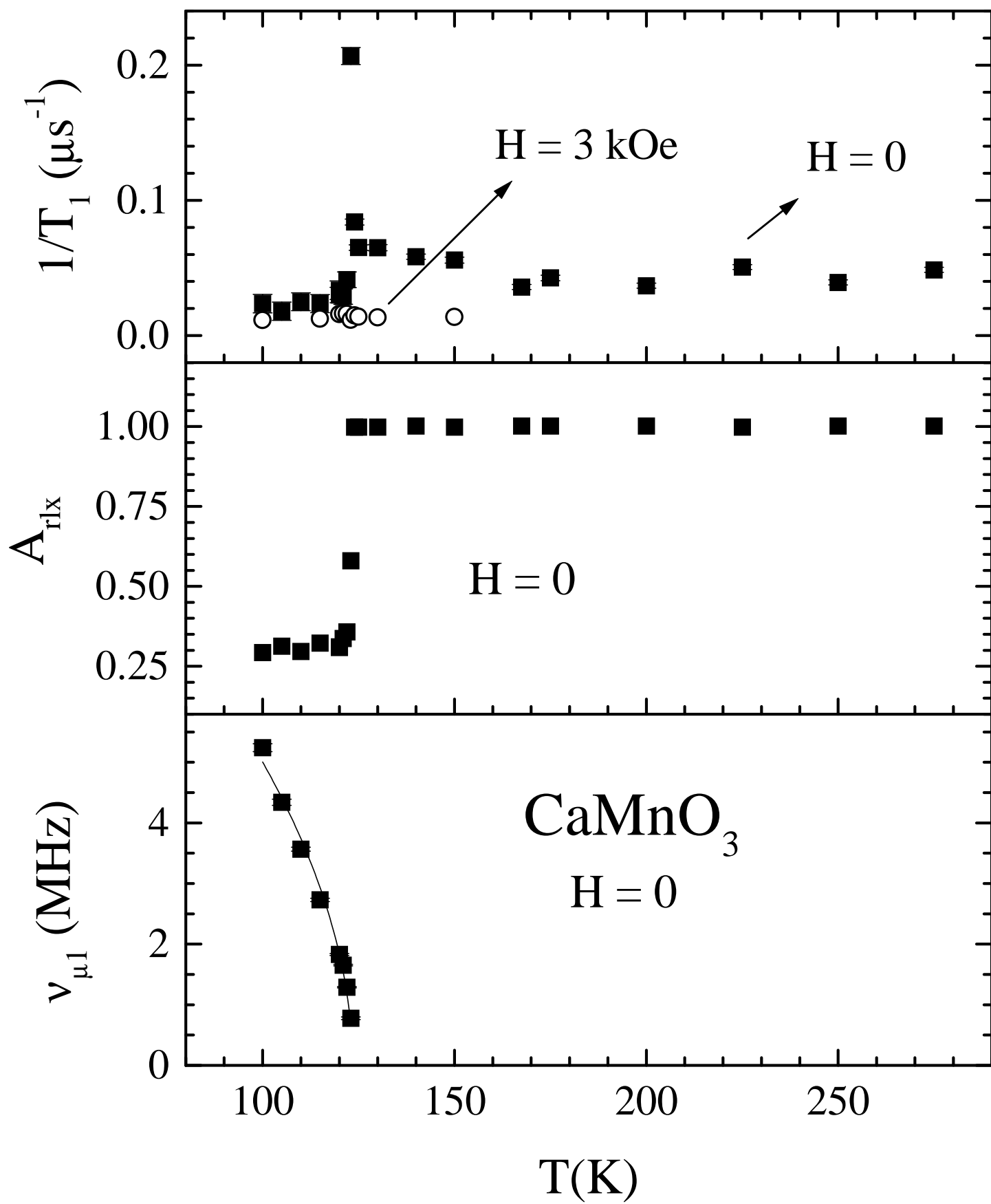
FIG. 16. Temperature dependence of the μ SR fast (λ_f , top) and slow (λ_s , bottom) spin-lattice relaxation rates for zero applied field in $\text{La}_{0.67}\text{Ca}_{0.33}\text{MnO}_3$ obtained from a fit to Eq. (3) [closed symbols, exponent $K \simeq 1$ in Eq. (3)] and Eq. (4) [open symbols].

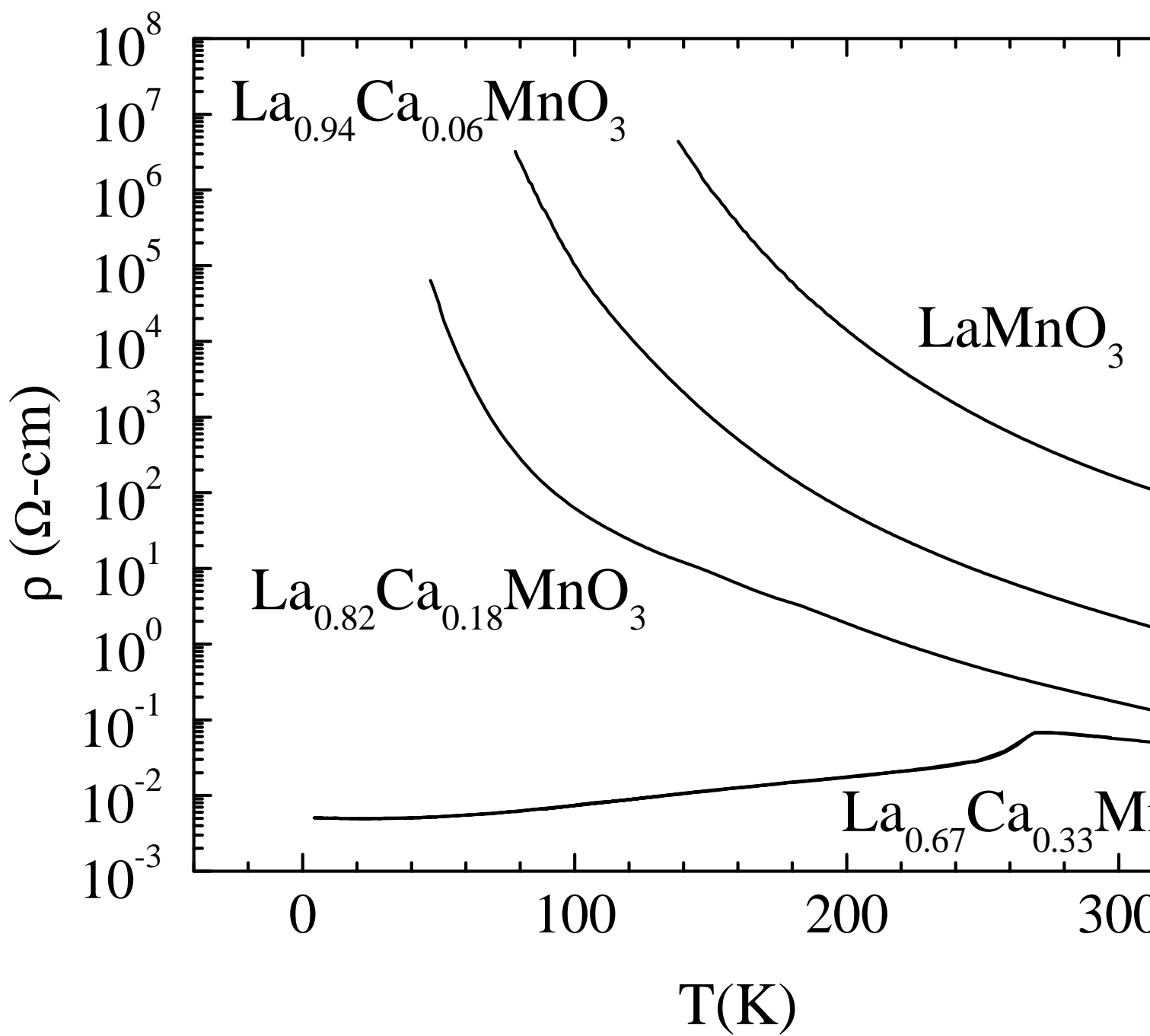
FIG. 17. Temperature dependence of the μ SR fast (A_f , top) and slow (A_s , bottom) amplitudes for zero applied field in $\text{La}_{0.67}\text{Ca}_{0.33}\text{MnO}_3$ and $\text{La}_{0.82}\text{Ca}_{0.18}\text{MnO}_3$ obtained from a fit to Eq. (3) [closed symbols, exponent $K \simeq 1$ in Eq. (3)] and Eq. (4) [open symbols].

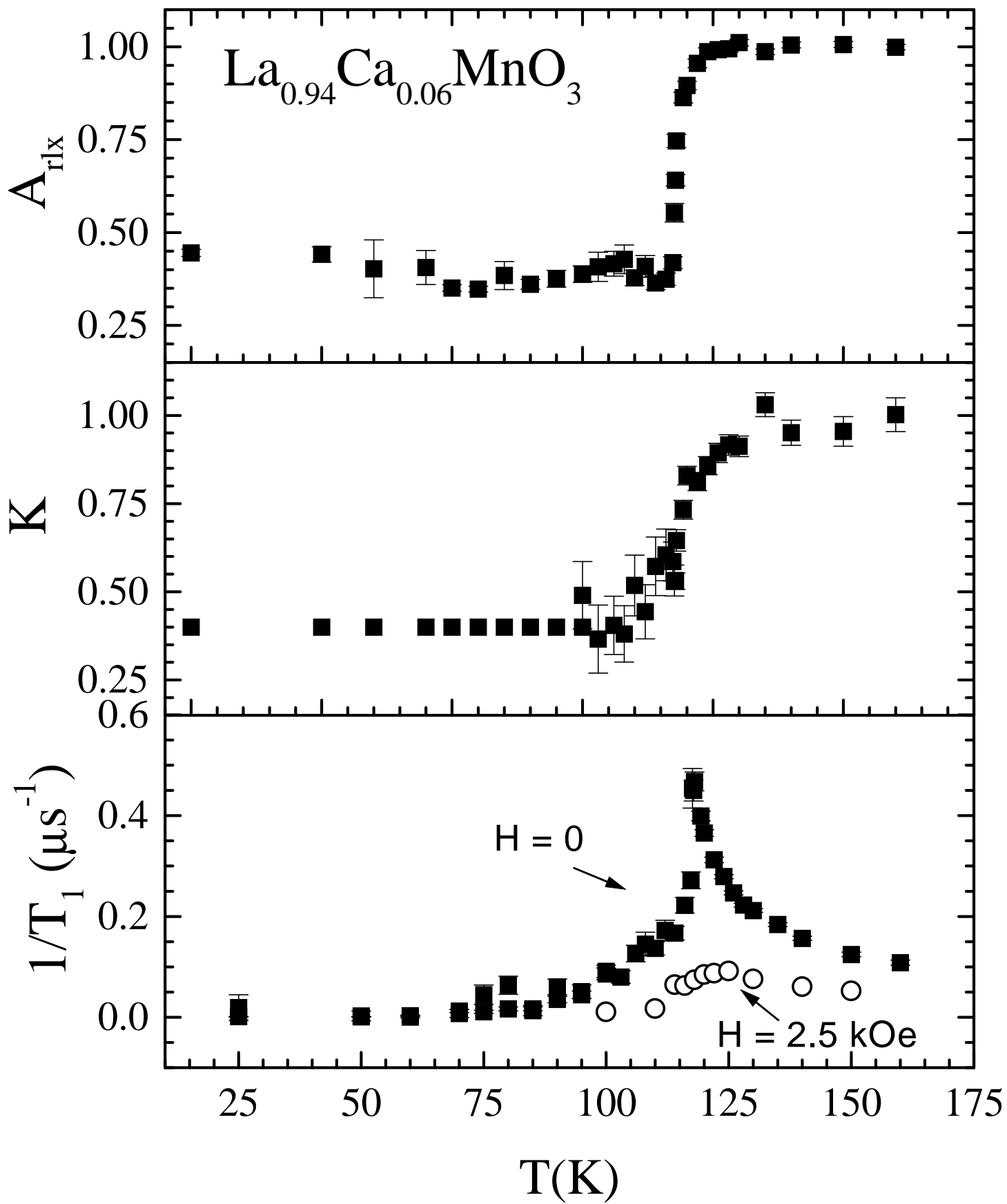


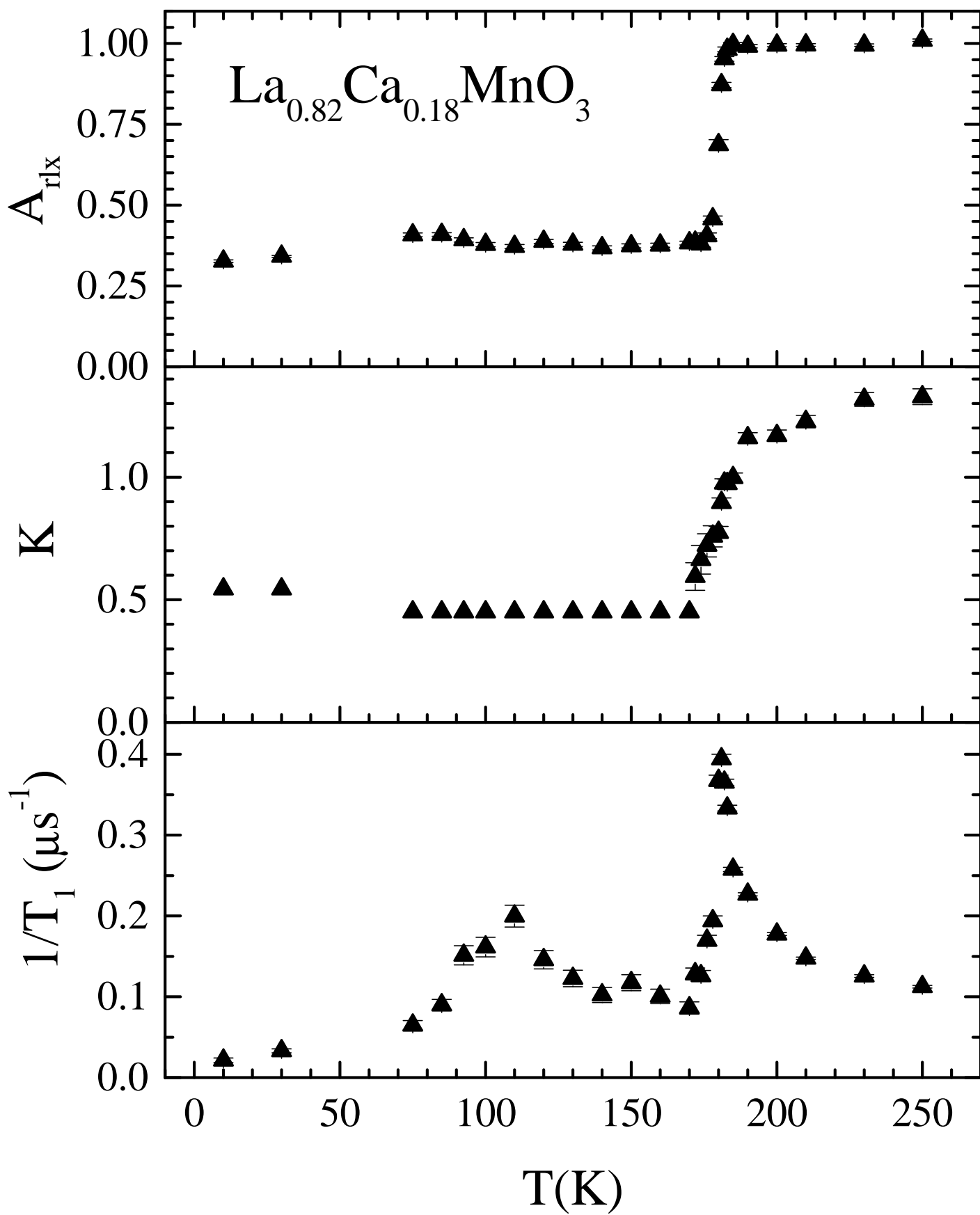


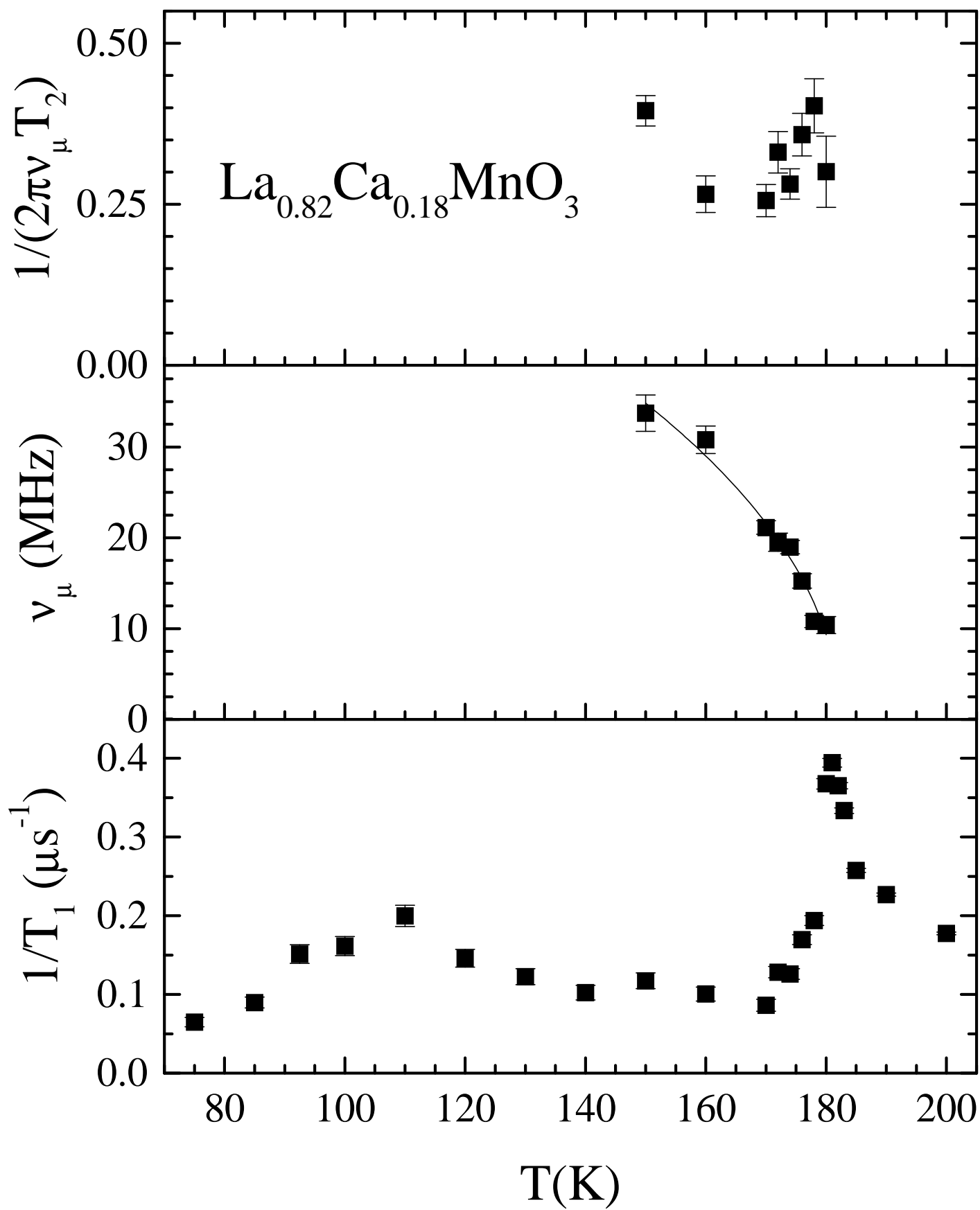


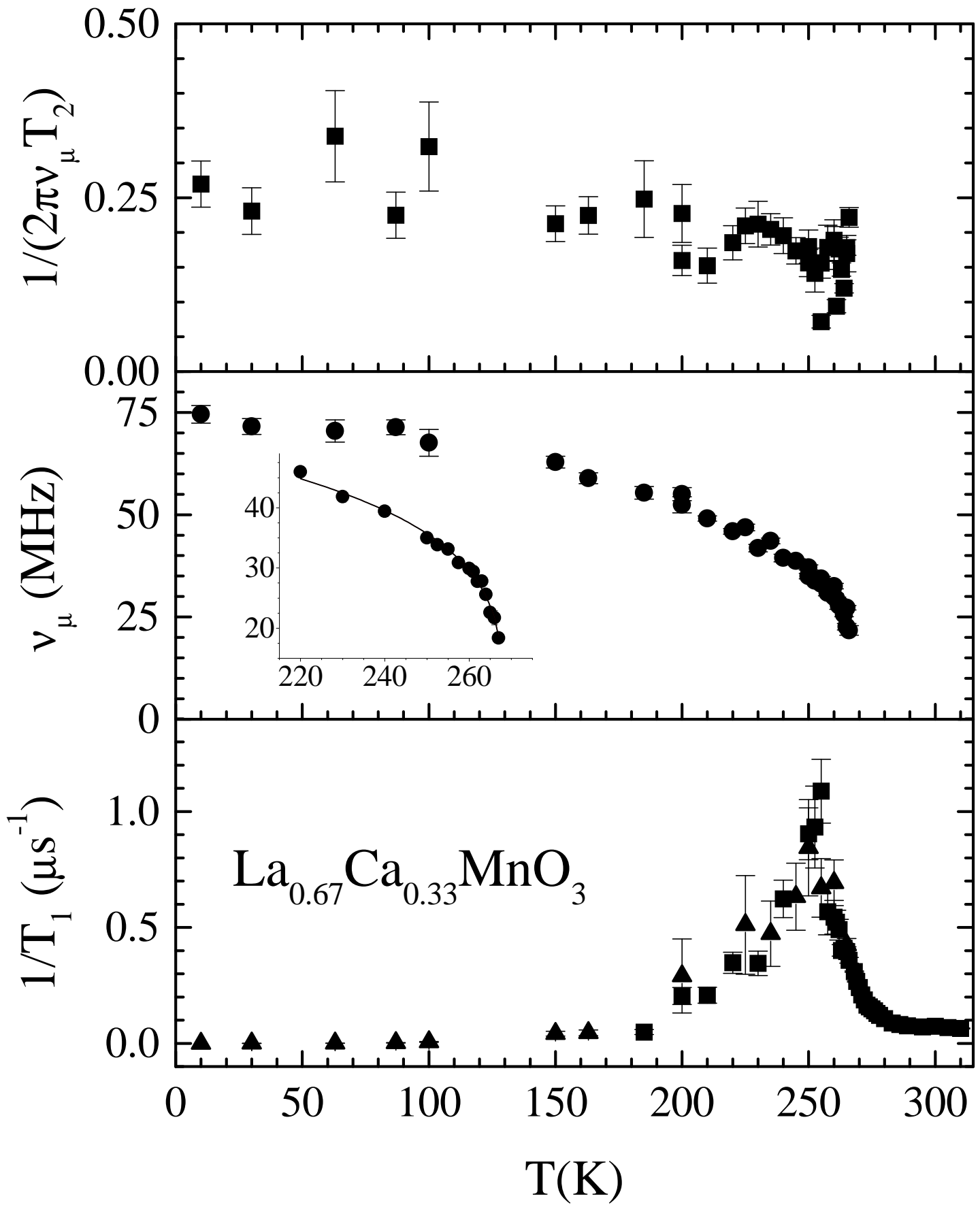


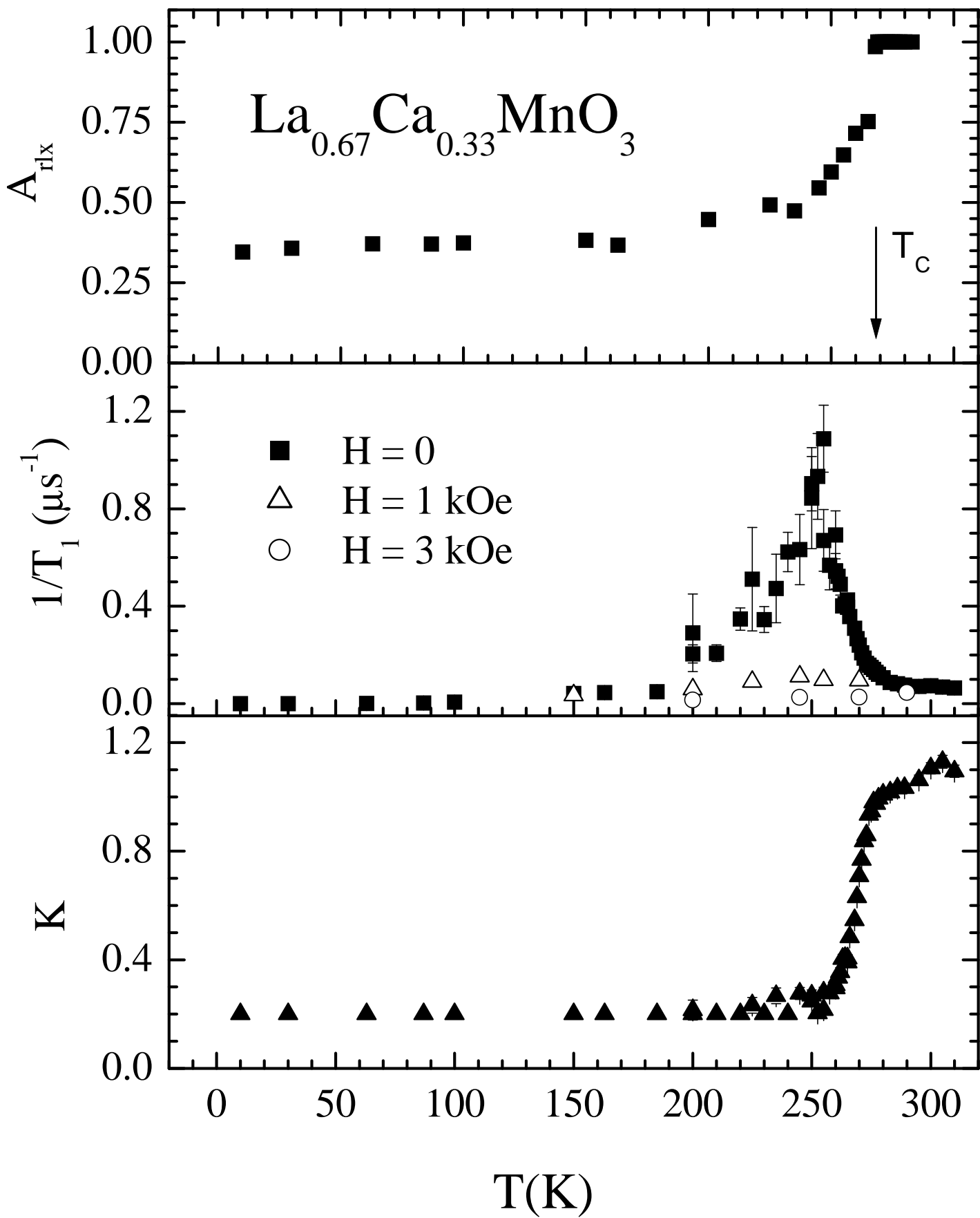












$\text{La}_{0.33}\text{Ca}_{0.67}\text{MnO}_3$

